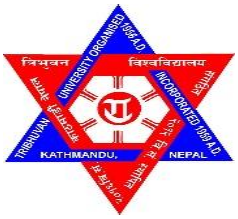

TRIBHUVAN UNIVERSITY

INSTITUTE OF ENGINEERING

PULCHOWK CAMPUS

Thesis no.: M-16-MSMSDE-2017/2019

Development of Mathematical Model of Magneto- Rheological Damper

by

Kushal Shrestha

A THESIS

SUBMITTED TO THE DEPARTMENT OF MECHANICAL ENGINEERING

IN PARTIAL FULFILLMENT OF THE REQUIREMENTS FOR THE

DEGREE OF MASTER OF SCIENCE IN

MECHANICAL SYSTEMS DESIGN AND ENGINEERING

DEPARTMENT OF MECHANICAL ENGINEERING

LALITPUR, NEPAL

NOVEMBER, 2019

COPYRIGHT

TRIBHUVAN UNIVERSITY

INSTITUTE OF ENGINEERING

PULCHOWK CAMPUS

DEPARTMENT OF MECHANICAL ENGINEERING

The undersigned certify that they have read, and recommended to the Institute of Engineering for acceptance, a thesis entitled "Development of Mathematical Model of Magneto- Rheological Damper" submitted by Kushal Shrestha in partial fulfillment of the requirements for the degree of Master in Mechanical Systems Design and Engineering.

_____

Supervisor, Dr. Mahesh Chandra Luitel

Associate Professor

Pulchowk Campus, Institute of Engineering

_____

Supervisor, Dr. Ajay Kumar Jha

Associate Professor

Pulchowk Campus, Institute of Engineering

_____

External Examiner, Dr. Bibek Baral

Professor

Kathmandu University

_____

Committee Chairperson, Dr. Nawaraj Bhattarai

Head of Department

Mechanical Engineering Department

_____

Date: November 8, 2019

ABSTRACT

Dampers are an important part of a vehicle suspension, which dissipate the energy of the motion of the suspension as thermal energy. A mathematical model can be an important tool in the understanding and design of a damper. A mathematical model of a twin tube damper was developed to represent the physical behavior of the damper and predict the force as a function of velocity. The model has included the provision of explicitly defining the viscosity of the damper system which will enable the model to accommodate the changes that may occur in the design. This also enables to calculate the variation of force with the change of viscosity which is the case of MR dampers. The model produced results concurrent with that available in literature.

The viscosity change for the MR damper for the change in current excitation applied to it has been predicted. The results show that when a current of 0.5 A is applied, magnetic flux of 0.002 T is induced. This results in a viscosity of 0.4 Pa.s. In comparison, the viscosity of MR fluid not subjected to magnetic field has a typical viscosity of about 0.11 +/- 0.02 Pa.s.

When this viscosity and its variation is applied to the model a 29% increase in damping force has been calculated, over the range of 0 to 0.5 A, with a maximum of 138 N obtained for the damper with a mechanical excitation of amplitude 20 mm and frequency of 2 Hz. The results obtained through the model have been compared with the experimental results found in literature for validation and the comparison has shown that the results are appropriate.

ACKNOWLEDGEMENT

I am thankful to the Department of Mechanical Engineering, Pulchowk Campus, for providing the prospect of conducting my thesis.

I owe my gratitude to my respected supervisors Asso. Prof. Dr. Mahesh Chandra Luitel and Asso. Prof. Dr. Ajay Kumar Jha for their untiring effort towards mentoring, guiding and supporting my thesis. Without their valuable suggestion and advices this thesis would have been impossible.

I also express my deepest appreciation to Campus Chief and Program Coordinator for MSc. in Mechanical Systems Design and Engineering Prof. Dr. Laxman Poudel and Head of Department, Asso. Prof. Dr. Nawaraj Bhattarai who have continuously supported me in my thesis and provided me courage and hope throughout the project.

I am thankful to Deputy Head of Department, Asso. Prof. Hari Dura for his expertise and support throughout the study. I would also like to thank Mr. Janak Kumar Tharu whose valuable insights helped me throughout the duration of the study

Finally, I want to thank all the members of Mechanical Systems Design and Engineering for their support.

TABLE OF CONTENTS

LIST OF TABLES

LIST OF FIGURES

LIST OF ABBREVIATIONS

CFD	Computational Fluid Dynamics
CVP	Continuous Velocity Plot
DC	Direct Current
ER	Electro- Rheological
MR	Magneto- Rheological
SIMPLE	Semi-Implicit Method for Pressure-Linked Equations

CHAPTER ONE: INTRODUCTION

1.1 Background

The suspension system is an important element of a vehicle. It is essential to provide the required handling to the vehicle as well as to provide a comfortable ride quality to the passengers. The irregularities in the surface of the road induces vibration in the moving vehicle, which reduces passenger comfort. Furthermore, the displacement of wheels during such vibrations may cause the wheels to loose contact with the road surface, which may lead to a loss of control of the vehicle. The suspension system is made of components like tires, springs (stiffness element), shock absorbers or dampers (dissipation elements) and linkages and employs them to obtain its objectives. Springs support the weight of the vehicle and absorb additional load by compressing. The dissipation element or the shock absorber dissipate the kinetic energy imparted to it due to the road surface as thermal energy of the fluid by forcing the fluid through different orifices.

The comfort and safety of passengers travelling in a vehicle can be improved by minimizing the body vibration caused during different road conditions and maneuvers of the vehicle and can be achieved using suspension systems. A variety of stiffness element like coil springs, leaf springs and a variety of dissipation components and their numerous combinations result in a large number of possible suspension system.

The dampers lower the amplitude and/or the frequency of vibration. Dampers are classified as “hard” or “soft” and each has their own use. The hard dampers provide better traction and stability and are used when control is paramount like in vehicles, which have to maneuver at high speeds, or vehicles, which need to carry very heavy loads. The soft dampers are used in vehicles, which are designed for providing maximum comfort and their use results in reduced bumpiness of the vehicle. Their choice depends on the type of vehicle and their intended use. Their use is chosen by conducting a vibration analysis of the vehicle by employing the stiffness and damping characteristics of the suspension system into the model of the vehicle. During the working of the damper, the suspension travels up and down, the hydraulic fluid is force through orifices, which slows the suspension motion. Based on construction, dampers are either twin tube or monotube and their variations. Basically, twin tube dampers stores the oil that is displaced by the piston rod when entering the cylinder in a remote

oil chamber and the monotube dampers use a floating piston that operated against a gas chamber whose size varies due to compression or expansion.

The suspension system can be broadly classified into three categories namely active, semi-active and passive systems. The differentiating characteristics of these systems are the amount of energy needed for their operation and the adaptability of the suspension system to the road conditions. In active systems, actuators are used to control the relative movement of the wheels and the chassis such that the chassis is raised or lowered independently to the wheels, while in passive systems the movement is determined completely by the road surface. The passive systems face the problem of maintaining the right contact with the road which requires "stiff" suspension, while also absorbing the road disturbances for which a "soft" suspension is needed. The semi-active systems change the parameters of the suspension system by using external power relatively lower than that needed in active systems. These systems continue to function as the passive system when the external power is interrupted so it can be regarded as having a "fail-safe" option.

Semi-active control devices offer reliability comparable to that of passive devices while providing the adaptability comparable to active systems but at reduced power requirements. The damping is tuned in real time but instead of injecting energy into the controlled system, the semi-active suspension uses different strategies to control the damping parameter. As a method to control damping, the orifice through which the damping fluid is to pass may be changed hence changing the force required to push the fluid through the orifice. Similarly, the property of the fluid itself may be altered by application of electric or magnetic fields. In case of Electro-Rheological (ER) dampers, electrical field of the magnitude of 1-5 kV is applied to the damping fluid which increases the viscosity and consequently damping coefficient of the fluid. The ER dampers suffer from the requirement of high voltage but in addition have an intolerance to impurities and a small operating temperature range. Magneto-Rheological (MR) dampers use magnetic field to alter the viscosity of the damping fluid. It uses a special type of fluid, which contains micron sized ferromagnetic particles suspended in oil. When the magnetic field is applied to the fluid, the particles get arranged along the path of the magnetic field. Once they are arranged in this manner, they resist being moved out of their respective flux lines and act a barrier to fluid flow.

1.2 Statement of Problem

The comfort of a passenger in a vehicle is of very high importance. This critical function is carried out by the suspension system of the vehicle. The most common type suspension system is the passive type but due to the lack of adaptability, the passive suspension system cannot provide the balance between maneuverability and comfort. So, in order to introduce adaptability, semi-active damper may be used instead of passive dampers. The passive type suspension system has been extensively studied but the mathematical model of MR damper; a semi-active damper has not been studied. So, this study will focus on developing the mathematical model of a damper with a provision to accommodate the properties of MR fluid.

1.3 Objectives

1.3.1. Main Objective

The main objective of this study is to develop mathematical model of Magneto-rheological damper.

1.3.2. Specific Objectives

- To develop mathematical model for twin-tube passive damper.
- To conduct magnetic analysis on damper model with the properties of MR fluid.
- To develop mathematical model of twin-tube damper with the properties of MR fluid.

1.4 Scope

The scope of this study is to develop a mathematical model of Magneto-rheological damper by introducing the properties of MR fluid in a commercially available twin-tube damper and compare the results with that obtained through literature. This will provide a basis for study of application of MR damper.

1.5 Limitations

- The study will not consider the temperature changes within the damper.
- The study will be based on data available through literature.
- The validation of results will be limited to validation through literature.

CHAPTER TWO: LITERATURE REVIEW

2.1 Earlier Research

2.1.1. Types of Suspension system

Different type of suspension systems has been studied and are currently available. Passive suspension systems are conventional systems which work by storing energy in the spring element and dissipating it through the damper. The parameters of such a system are fixed. A semi-active suspension used small amount of to change characteristics of the passive suspension system such as the damping constant. A greater control of the suspension system can be obtained by employing active systems, which introduces energy to the system and apply force as required to counter the road excitation.

The main purposes of vehicle suspension system include maintaining proper contact with road surface and reducing the effect of shock forces. (Rill, 2012).The passive suspension systems are either "soft" as in luxury cars, which can absorb the road disturbances or "stiff" which is required to maintain proper road contact. One of the either properties is sacrificed when using passive systems according to the type of the vehicle (Kashem et al., 2018). A system which has high damping characteristics performs well in the range of the resonant frequency but the performance is poor in other frequency ranges while on the contrary a system with low damping behaves the opposite. (Rao, 2011). A simulation was run to compare the behavior of semi-active suspension systems with passive suspension systems for a quarter car model, which concluded than using semi-active systems lead to an almost total elimination of the system oscillations, a reduction in the amplitude of the oscillatory phenomena and a reduction is disruptive time, which is of great advantage (Mihai & Andronic, 2014).

When evaluated for road profiles of short wavelength and with cleats, semi-active suspension system can match the performance of active suspension system without bottoming of suspension or road separation while limiting energy and size requirements. Hence, semi-active dampers can be used as a substitute of active suspension system at reduced power consumption, cost and complexity as well as with greater reliability (Siramdasu & Taheri, 2017).

There are three types of semi-active suspension systems commonly available namely Position Controlled Valves, Electro-rheological (ER) dampers and Magneto-rheological (MR) dampers. Of these, the Position Controlled Valves are expensive and have slow response rates while the ER dampers suffer from the requirement of very high voltages (1-5 kV) and having a very narrow working temperature range. On the contrary, ME dampers use MR fluid and magnetic flux and can produce response rates of less than 10 milliseconds and minimal power usage (typically 12V, 1A max current) (K., A., Kumar, & Gangadharan, 2014) (Tyagi, 2016). The operating temperature range for ionic, Direct Current (DC) ER dampers is +10 to 90 ℃ and cannot tolerate impurities. In contrast MR dampers can work between -40 ℃ and +150 ℃ and they are unaffected by most impurities (Guglielmino et al., 2008)

ER and MR fluids are controllable fluids made by mixing fine particles into a liquid with low viscosity. When high electric field or magnetic field is applied to the fluid, the particles form chain-like fibrous structures. When the electric field or magnetic field reaches certain strength, the suspensions will solidify and exhibit high yield stress. This is a reversible process and the suspension is liquefied after removal of the field. The time for this property change is less than a few milliseconds. Hence, the process is quick and controllable. (Yao et al., 2002)

2.1.2. Existing Mathematical Models

Various researchers have worked on mathematical models to depict the working of a damper. Notably, (Talbott & Starkey, 2002) presented a method to model a mono-tube damper and incorporated the different flows present in the working of the damper and force generated at different components of the damper. This study has been one of the basis for further study by other researchers.

(Meissen, 2009) had developed a mathematical model for a modern twin tube damper. The researcher had used the equations developed by (Talbott & Starkey, 2002). These models rely on experimentally determined coefficients to function. This restricts the adaptability of model developed for one model of the damper to the other damper.

2.1.3. Model of MR Damper

Many researchers have worked to correctly explain the behavior of MR fluids and have presented various models. The stress- strain behavior of the Bingham visco-plastic model has been used by (Spencer Jr., Dyke, Sain, & Carlson, 1997) to describe the

behavior of MR fluids. The plastic viscosity has been described as the slope of the measured shear stress versus shear strain rate data. For positive values of the shear-rate $\dot{\gamma}$, the total stress is given by:

$$\tau = \tau_{y(field)} + \eta\dot{\gamma} \qquad \text{Equation 2.1}$$

where, $\tau_{y(field)}$ is the yield stress induced by the magnetic field and η is the viscosity of the fluid. (Shames & Cozzarelli, 2014)

$$F = f_c\, sgn(\dot{x}) + c_0 + f_0 \qquad \text{Equation 2.2}$$

where, c_0 is the damping coefficient and f_c is the frictional force (related to fluid yield stress. A schematic of Bingham model is shown in Figure 2-1:

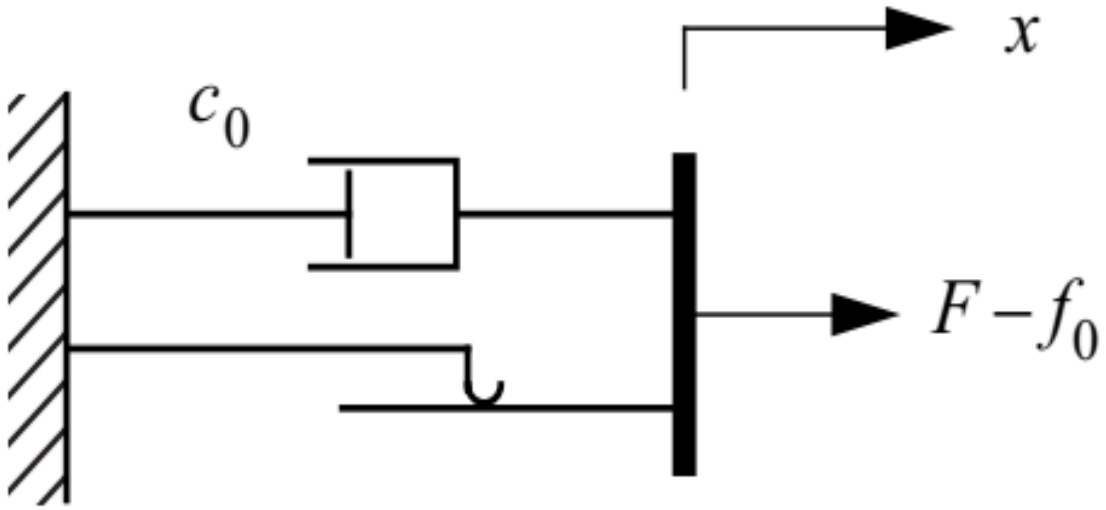

Figure 2-1: Bingham Model of a Controllable Fluid Damper

(Spencer Jr. et al., 1997)

Bouc-Wen model has also been used to model hysteretic systems and is extremely versatile. The system is schematically shown in Figure 2-2:

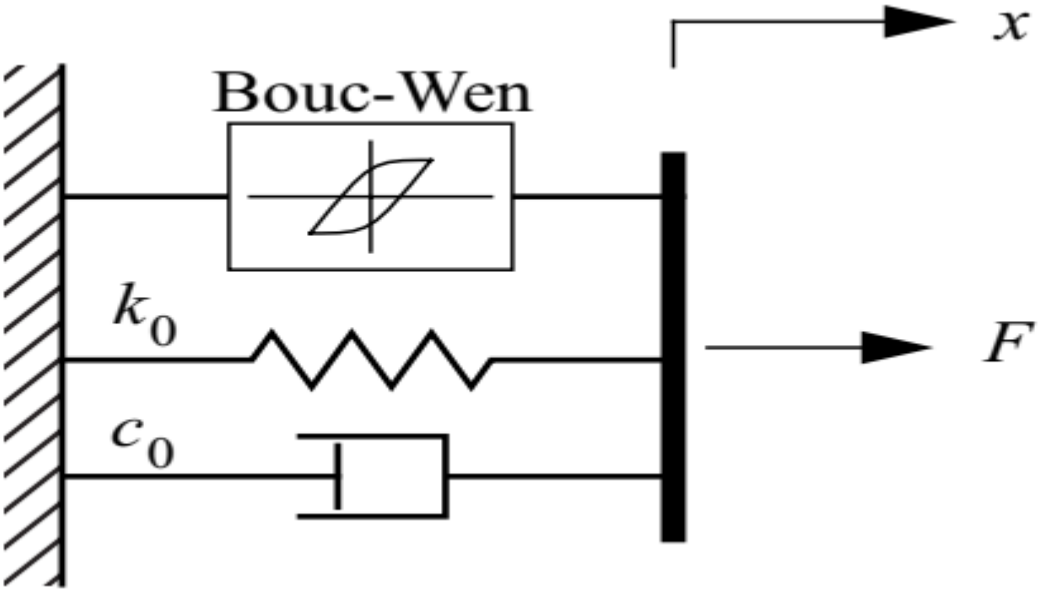

Figure 2-2: Bouc-Wen model of the MR Damper

(Spencer Jr. et al., 1997)

The force in the system is given by:

$$F = c_0\dot{x} + k_0(x - x_0) + \alpha z \qquad \text{Equation 2.3}$$

where, z is the evolutionary variable governed by:

$$\dot{z} = -\gamma|\dot{x}|z|z|^{n-1} - \beta\dot{x}|z|^n + A\dot{x} \qquad \text{Equation 2.4}$$

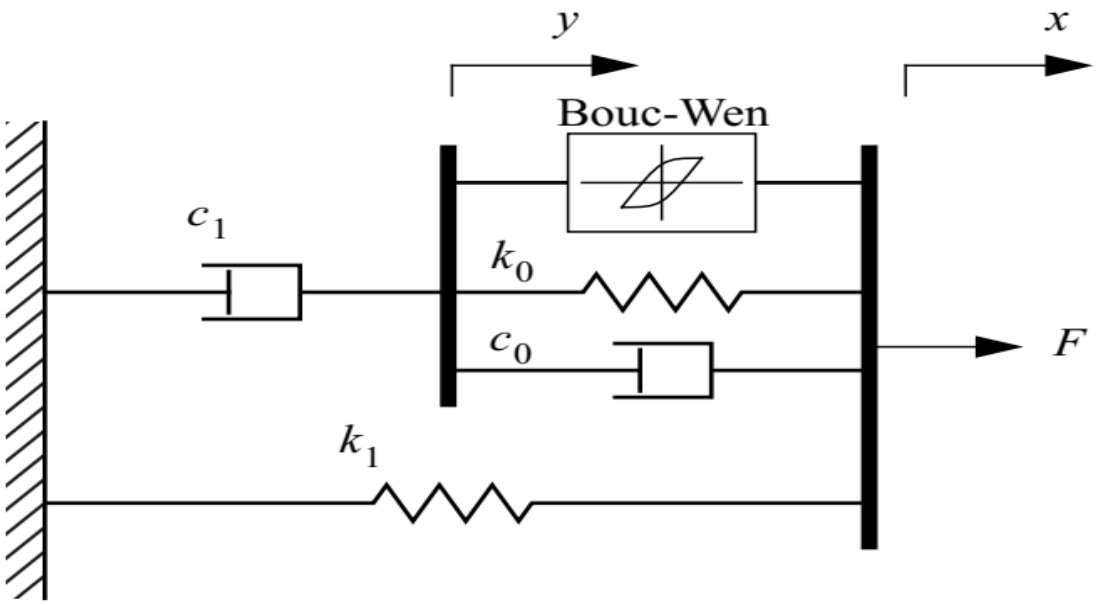

Figure 2-3: Modified Bouc-Wen Model

(Spencer Jr. et al., 1997)

Modification was done to the original Bouc-Wen model to better represent the region where the acceleration and velocity have opposite signs and the magnitude of the velocities are small. The proposed model is as shown in Figure 2-3.

The model has been generalized for fluctuating magnetic fields as

Force:

$$c_1\dot{y} = \alpha z + k_0(x - y) + c_0(\dot{x} - \dot{y}) + k_1(x - x_0) \qquad \text{Equation 2.5}$$

and the evolutionary variable z is given by:

$$\dot{z} = -\gamma|\dot{x} - \dot{y}|z|z|^{n-1} - \beta(\dot{x} - \dot{y})|z|^n + A(\dot{x} - \dot{y}) \qquad \text{Equation 2.6}$$

the parameters are modified as

$$\alpha = \alpha(u) = \alpha_a + \alpha_b u, c_1 = c_1(u) = c_{1a} + c_{1b}u \qquad \text{Equation 2.7}$$

and,

$$c_0 = c_0(u) = c_{0a} + c_{0b}u$$

and

$$\dot{u} = -\eta(u - v) \qquad \text{Equation 2.8}$$

where, v is the voltage applied to the damper.

Through optimization, following optimum parameters were obtained:

Table 2.1: Parameters for Generalized Model

(Spencer Jr., Dyke, Sain, & Carlson, 1997)

Parameter	Value	Parameter	Value
c_{0a}	21.0 N.sec/cm	α_a	140 N/cm
c_{0b}	3.50 N.sec/cm.V	α_b	695 N/cm.V
k_0	46.9 N/cm	γ	363 cm^{-2}
c_{1a}	283 N.sec/cm	β	363 cm^{-2}
c_{1b}	2.95 N.sec/cm. V	A	301
k_1	5.00 N/ cm	n	2
x_0	14.3 cm	η	190 sec^{-1}

Another approach taken to predict the behavior of the MR damper is to use curve fitting to the experimental data. (Ashfak et al., 2013) have used this method to predict the behavior with good accuracy. They used two experimentally developed relations, one

for fluid shear stress in terms of magnetic field and another for viscosity in terms of shear rate. Then by combining the effects of shear and viscosity, they have obtained a variation of force with velocity.

2.1.4. Material Properties of MR fluid

MR fluid is a colloidal suspension of polarized particles. The carrier fluid is usually mineral or silicon oil which combines low tendency to evaporation with resistance to temperature. Micro-magnets are distributed in the carrier oil. The control of the damping properties of the damper is done by controlling the feed current. The time necessary to obtain 90% of the final viscosity of the MR fluid at a given strength of the magnetic field is of the order of microseconds. (Roszkowski et al., 2008)

Lords Corporation is a pioneer in the field of Magnetorheological fluid and their application in dampers and the properties they have published have been used repeatedly in a large number of studies. In the data sheet, (MRF-132DG Magneto-Rheological Fluid, 2018) ; provide by Lords Corporation, the properties of the MR Fluid is given. In the data sheet, it describes the working of MR damper. The damper behaves as a passive damper in which the damper fluid flows freely in the absence of the magnetic field. However, when the damper is subject to magnetic field, the suspended particles align in the direction of the field in chain like fashion, which restricts the fluid's motion through the opening and valves provided within the damper. The properties of the MR fluid is given below:

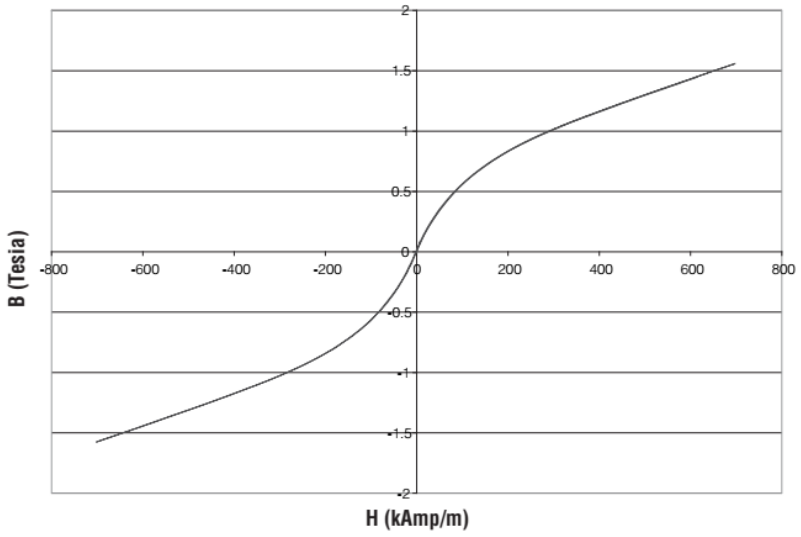

Figure 2-4: Properties of MR Fluid

(Source: (MRF-132DG Magneto-Rheological Fluid, 2018))

The density is in the range of 2.95- 3.15 g/cm^3 and the viscosity is 0.112 ± 0.02 Pa s.

2.1.5. Magnetisation in MR damper

(Raghu & Ramji, 2018) during their study of MR dampers, used AWG 24-gauge copper to induce magnetic field in the MR fluid. The study was done to understand the aspects of material selection, geometry design and magnetic circuit design. In the magnetic circuit design process, the current excitation was provided. So in order to provide the required current excitation, the appropriate conductor must be used. For this AWG 24-gauge copper wire was used which has low resistance.

(Roszkowski et al., 2008) by applying a method of indirect measurement using a reference fluid of known properties graphically depicted the dependence of viscosity of magnetic fluid with the magnetic field induced upon it. The graph is shown in Figure 2-5:

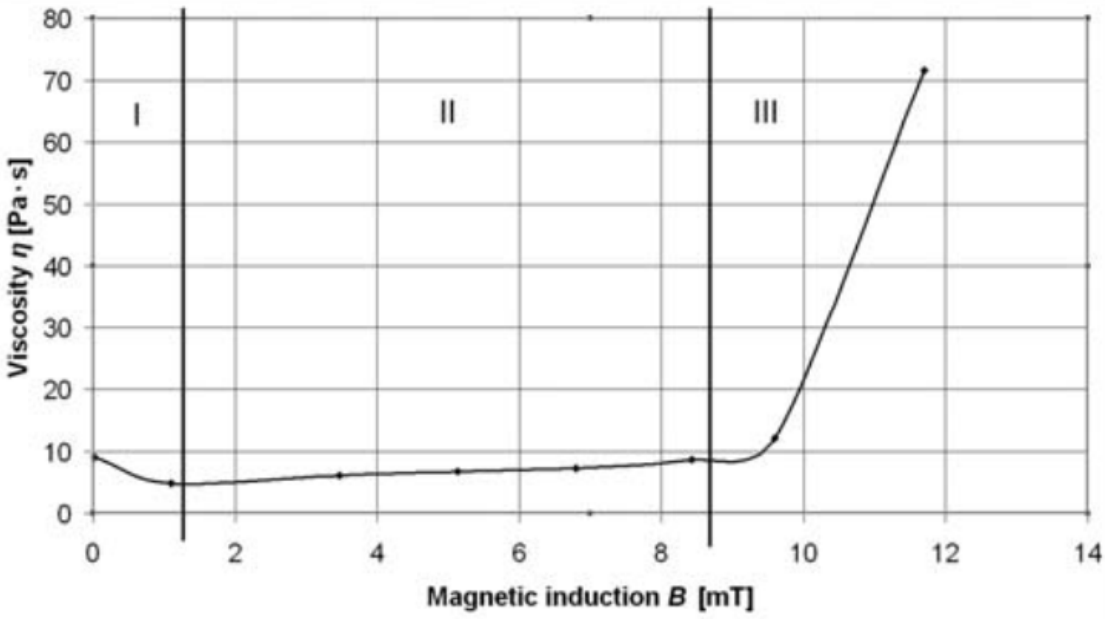

Figure 2-5: Viscosity vs Magnetic induction

(Roszkowski, et al., 2008)

Similarly, (Premalata, Chokkalingam, & Mahendran, 2012) have conducted an experiment to find out how the variation in properties of the MR fluid occurs due to different factors. Two graphs have been presented one of which represent the relation between viscosity and shear rate and the other presents the shear stress variation with magnetic field strength as shown in Figure 2-6 and Figure 2-7.

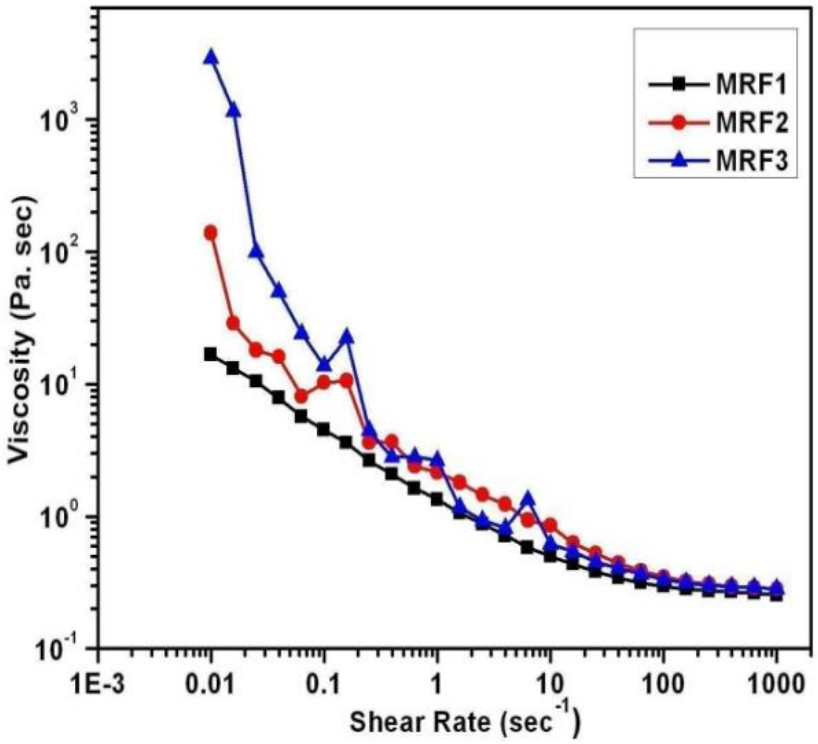

Figure 2-6: Relationship between Viscosity and Shear Rate

(Source: (Premalata, et al., 2012))

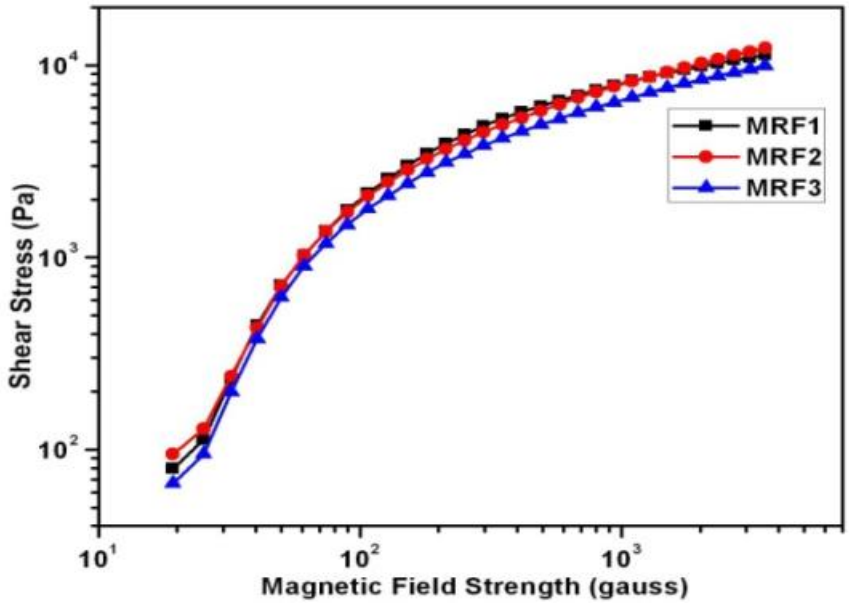

Figure 2-7: Variation of Shear Stress with Magnetic Field Stregth

(Source: (Premalata, et al., 2012))

2.2 Research Gap

Although various studies have provided a mathematical model to determine the performance of monotube damper, work still remains to be done in the case of twin tube damper. Also, the modeling of MR dampers have been limited to experimental curve fitting or equivalent models. So further research needs to be done in developing a model of the twin tube damper and evolving it to accommodate the MR damper characteristics.

CHAPTER THREE: RESEARCH METHODOLOGY

The research was conducted in the following steps:

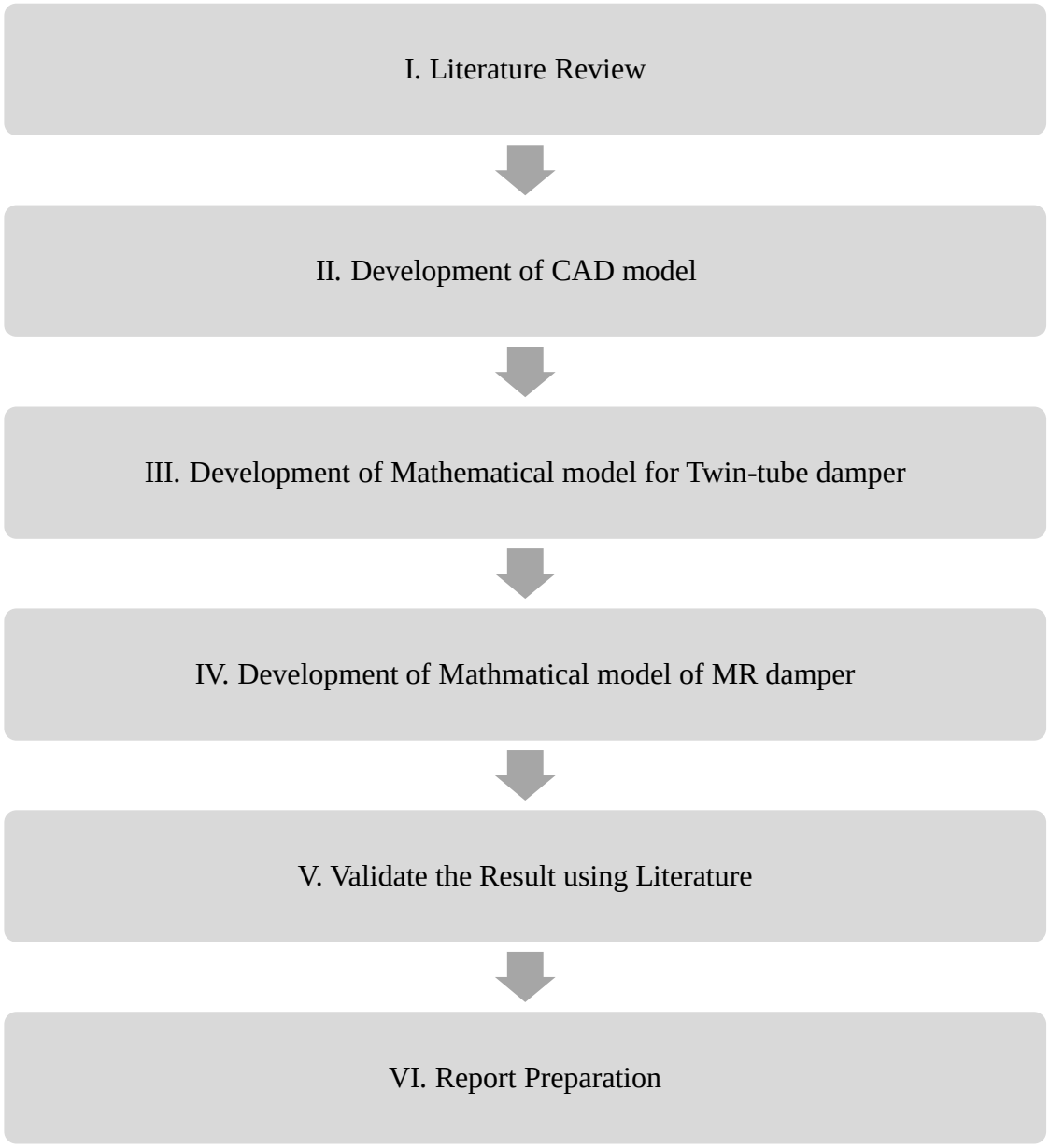

I. Literature Review:

This was a continuous process of acquainting with the available knowledge in the relevant field. It was done to find the research gap and summarize the results of study conducted over the years. This helped guide the thesis and helped to make judgement regarding the decisions throughout the thesis. Literature review was done to find results of similar study for comparison. This was taken as the basis to validate the results obtained through this study.

II. Development of CAD model:

Damper available in the market was broken down to develop CAD models using CATIA. This was done to understand the damper working and construction of the damper. In doing so, the detail parameters of the damper will be obtained. This will also provide a basis for development of mathematical model and simulation.

III. Development of mathematical model of Twin-tube damper

On the basis of the CAD model, the model of the twin-tube damper was created. The working of the damper and flow pattern were considered for this. The results obtained from the model were analyzed and compared with the results available through literature for similar dampers. A one-eight model of rebound valve of the damper was created using ANSYS and it was simulated as a means of further validate the results obtained through the mathematical model.

IV. Development of Mathematical model of MR damper:

The properties of MR fluid are applied to the damper. For activation of MR damper properties, magnetic field needs to be applied. So the effect of introducing magnetic field to the MR fluid was analyzed in the form of magnetic field induced in it. The external magnetic field was applied as a function of current as per the limits set forth in various literature. The induced magnetic field determine the property the MR fluid exhibits at that input current value. So by changing these properties in the mathematical model, the variation in force produced by the damper was analyzed.

V. Validation of Results obtained through literature:

The results obtained through the model for Twin-tube damper and the MR damper were validated using the experimental results available in literature.

VI. Prepare a report:

The results of the analysis was analyzed and consolidated. The findings along with the problems and limitations is presented in the report.

3.1 Damper Parameters

For the damper model, a damper was obtained and used as reference. The damper was broken down and a CAD model was created using CATIA by measuring the different components of the damper. The damper was measured with a precision of 0.01 mm for linear dimensions. The relevant dimensions of the model are tabulated in Table 3.1:

Table 3.1: Dimensions of CAD Model

Dimension	Value
Extended Length	651 mm
Stroke	243.58 mm
Bore	13.5 mm
Diameter of oil passage in Compression Valve	2 mm
Length of oil passage in Compression Valve	6.3 mm
Diameter of oil passage in Rebound Valve	6.5 mm
Length of oil passage in Rebound Valve	14.5 mm
Volume of oil in Damper (Approx)	31 ml

The damper was then altered so as to accommodate the coils and function as a MR damper. To convert it into a MR damper, a slot was provided in the Compression Valve of the damper. The sectional view of the damper is as shown below:

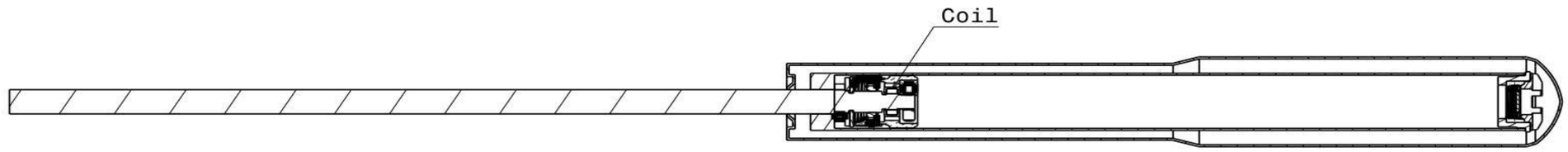

Sectional view with the Coil position of modified damper

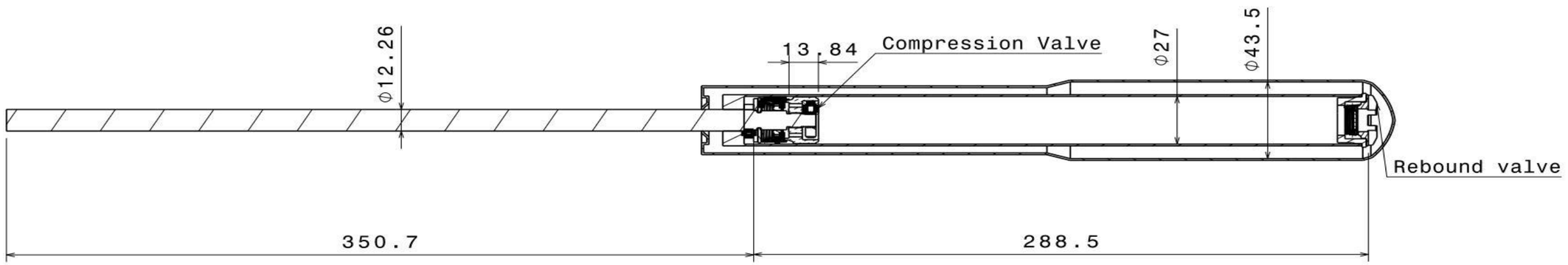

Sectional View of Original Damper

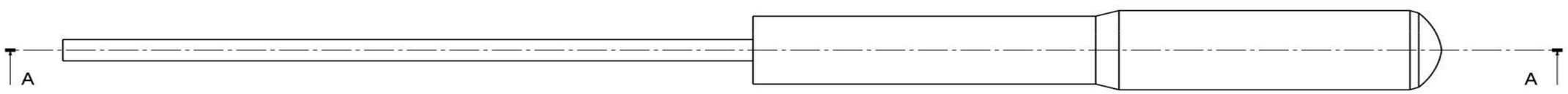

Front View of Original Damper
Scale: 1:2

3.2 Mathematical Model of Damper

3.2.1. Basic Equations

1. Flow Through Orifice

For a fluid passing through an orifice of cross sectional area, *A* with a velocity *v*, the mass flow rate of the fluid is given by:

$$Q = C_d A v$$

where, C_d is the steady state discharge coefficient which is the product of area coefficient and velocity coefficient. The fluid initially contract upon entering the orifice and then expands. The minimum cross section area of the fluid due to the contraction is called vena-contracta. The area coefficient is the ratio of cross sectional area at the vena-contracta to the geometric area of the orifice. A value of 0.8 for area coefficient is observed for most dampers (Dixon, 2007). Similarly, velocity coefficient is the ratio of theoretical exit velocity to the actual velocity. The steady state discharge coefficient, C_d can be taken as 0.7 (range of 0.6 to 0.8) for practical damper operating condition. Now, by applying boundary condition to the flow and considering the initial velocity as zero, we get:

$$v = \sqrt{\frac{2(P_1 - P_2)}{\rho}}$$

Therefore, by substituting the value of v, we get the mass flow rate as:

$$Q = C_d A \sqrt{\frac{2(P_1 - P_2)}{\rho}}$$

This equation has been used for the flow through orifice for developing the model of the damper.

2. Fully Developed Flow Through a Pipe:

For fluid passing through a pipe of diameter (D) caused due to pressure difference (ΔP) in the direction of the flow, the fully developed flow is given by:

$$Q = \frac{\pi \Delta P D^4}{128 \mu L}$$

The pipe has a length (L) and the fluid has a viscosity of (μ).

3. Fully Developed Flow between parallel plates:

If there exists a pressure gradient parallel to the plates, flow occurs between them and is represented as

$$\frac{Q}{l} = \frac{a^3 \Delta P}{12 \mu L}$$

Here, the flow occurs in the x-direction,

a is the distance between the plates,

L is the length of the plates in the direction of flow

ΔP is the pressure difference that governs the flow

l is the depth of the plate in the direction perpendicular to both a and L

This flow has been represented in the Cartesian coordinate system.

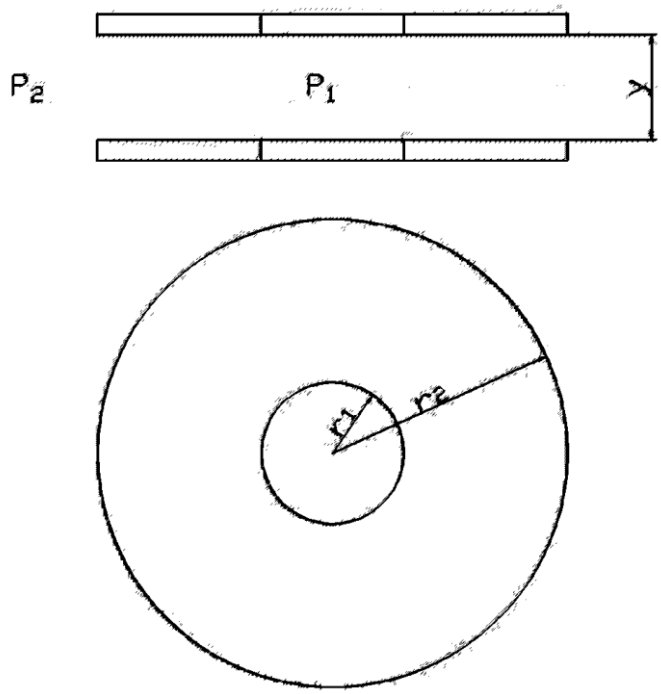

Figure 3-1: Flow between circular parallel plates

For circular plates as shown in Figure 3-1, the flow rate can be determined by using mass conservation and momentum conservation equations in cylindrical coordinates. The flow can be derived as:

We have, mass conservation equation:

$$\frac{1}{r}\frac{\partial(ru_r)}{\partial r}+\frac{1}{r}\frac{\partial u_\theta}{\partial \theta}+\frac{\partial u_z}{\partial z}=0$$

Momentum Conservation Equation:

r- component:

$$\rho\left(\frac{\partial u_r}{\partial t}+u_r\frac{\partial u_r}{\partial r}+\frac{u_\theta}{r}\frac{\partial u_r}{\partial \theta}-\frac{u_\theta^2}{r}+u_z\frac{\partial u_r}{\partial z}\right)$$
$$=-\frac{\partial P}{\partial r}+\rho g_r+\mu\left[\frac{1}{r}\frac{\partial\left(r\frac{\partial u_r}{\partial r}\right)}{\partial r}-\frac{u_r}{r^2}+\frac{1}{r^2}\frac{\partial^2 u_r}{\partial \theta^2}-\frac{2}{r^2}\frac{\partial u_\theta}{\partial \theta}+\frac{\partial^2 u_r}{\partial z^2}\right]$$

θ- component:

$$\rho\left(\frac{\partial u_\theta}{\partial t}+u_r\frac{\partial u_\theta}{\partial r}+\frac{u_\theta}{r}\frac{\partial u_\theta}{\partial \theta}+\frac{u_r u_\theta}{r}+u_z\frac{\partial u_\theta}{\partial z}\right)$$
$$=-\frac{1}{r}\frac{\partial P}{\partial r}+\rho g_\theta+\mu\left[\frac{1}{r}\frac{\partial\left(r\frac{\partial u_\theta}{\partial r}\right)}{\partial r}-\frac{u_\theta}{r^2}+\frac{1}{r^2}\frac{\partial^2 u_\theta}{\partial \theta^2}+\frac{2}{r^2}\frac{\partial u_r}{\partial \theta}+\frac{\partial^2 u_\theta}{\partial z^2}\right]$$

z- component:

$$\rho\left(\frac{\partial u_z}{\partial t}+u_r\frac{\partial u_z}{\partial r}+\frac{u_\theta}{r}\frac{\partial u_z}{\partial \theta}+u_z\frac{\partial u_z}{\partial z}\right)$$
$$=-\frac{\partial P}{\partial r}+\rho g_z+\mu\left[\frac{1}{r}\frac{\partial\left(r\frac{\partial u_z}{\partial r}\right)}{\partial r}+\frac{1}{r^2}\frac{\partial^2 u_z}{\partial \theta^2}+\frac{\partial^2 u_z}{\partial z^2}\right]$$

Assumptions:

$u_\theta = 0, u_z = 0$; for radial flow

$\frac{\partial u_r}{\partial \theta} = 0$; the velocity in θ direction is constant

$\vec{g} = 0$; neglecting body force

From mass conservation,

$$\frac{1}{r}\frac{\partial(ru_r)}{\partial r} = 0$$

or, $$\frac{r}{\partial r} = -\frac{u_r}{\partial u_r}$$

or, $$u_r = k/r$$

From z-component of Momentum conservation equation,

$$\frac{\partial P}{\partial z} = 0$$

From r-component of Momentum conservation equation,

$$\rho\left(u_r\frac{\partial u_r}{\partial r}\right) = -\frac{\partial P}{\partial r} + \mu\left[\frac{1}{r}\frac{\partial\left(r\frac{\partial u_r}{\partial r}\right)}{\partial r} - \frac{u_r}{r^2}\right]$$

Solving the equation, we get

$$\rho\left(u_r\frac{\partial u_r}{\partial r}\right) = -\frac{\partial P}{\partial r} + \mu\frac{\partial^2 u_r}{\partial z^2}$$

or, $$\rho\frac{k}{r}\left(\frac{k}{r^2}\right) = -\frac{\partial P}{\partial r} + \mu\frac{\partial^2\left(\frac{k}{r}\right)}{\partial z^2}$$

Integrating twice from $r = r_1$ to $r = r_2$

$$P_2 - P_1 = \frac{\rho(-k)}{2}\left(\frac{1}{r_2^2} - \frac{1}{r_1^2}\right) + \mu\left(\frac{\partial^2 k}{\partial z^2}\right)\ln\left(\frac{r_2}{r_1}\right)$$

Neglecting the nonlinear terms,

$$-\frac{\Delta P}{\rho} = \frac{\mu}{\rho}\left(\frac{\partial^2 k}{\partial z^2}\right)\ln\left(\frac{r_2}{r_1}\right)$$

Integrating twice with respect to z

$$\frac{\partial k}{\partial z} = -\frac{\Delta P}{\mu\ln\left(\frac{r_2}{r_1}\right)}z + c_1$$

$$k = -\frac{\Delta P}{\mu\ln\left(\frac{r_2}{r_1}\right)}\left(\frac{z^2}{2}\right) + c_1 z + c_2$$

By applying boundary conditions,

For $z = 0$, $v_r = 0 \therefore k = 0$ and $c_2 = 0$

For $z = a$, $v_r = 0 \therefore k = 0$

$$\therefore 0 = -\frac{\Delta P}{\mu \ln\left(\frac{r_2}{r_1}\right)}\left(\frac{a^2}{2}\right) + c_1 a$$

$$\therefore c_1 = -\frac{\Delta P}{\mu \ln\left(\frac{r_2}{r_1}\right)}\left(\frac{a}{2}\right)$$

So,

$$k = \frac{\Delta P}{\mu \ln\left(\frac{r_2}{r_1}\right)}\left(-\frac{z^2}{2} + \frac{az}{2}\right)$$

and,
$$u_r = \frac{\Delta P}{\mu r \ln\left(\frac{r_2}{r_1}\right)}\left(-\frac{z^2}{2} + \frac{az}{2}\right)$$

Since, volume flow rate is given as the product of area and velocity of flow, it can be found by:

$$Q = \int_{z=0}^{z=a} \frac{\Delta P}{\mu r \ln\left(\frac{r_2}{r_1}\right)}\left(-\frac{z^2}{2} + \frac{az}{2}\right)(2\pi r)dz$$

or,
$$Q = \frac{\pi a^3 \Delta P}{6\mu \ln\left(\frac{r_2}{r_1}\right)}$$

3.2.2. Flow of Damper Fluid

The schematic for fluid flow is shown in Figure 3-2. This shows the total flow that is possible. However, for the case of compression, Q_{vc} which is the flow from the compression chamber to the gas (or reservoir) chamber does not occur. Similarly, in rebound motion, the rebound piston valve flow, Q_{vr} is not allowed. So, the mathematical model for the case of rebound stroke and compression stroke will differ accordingly.

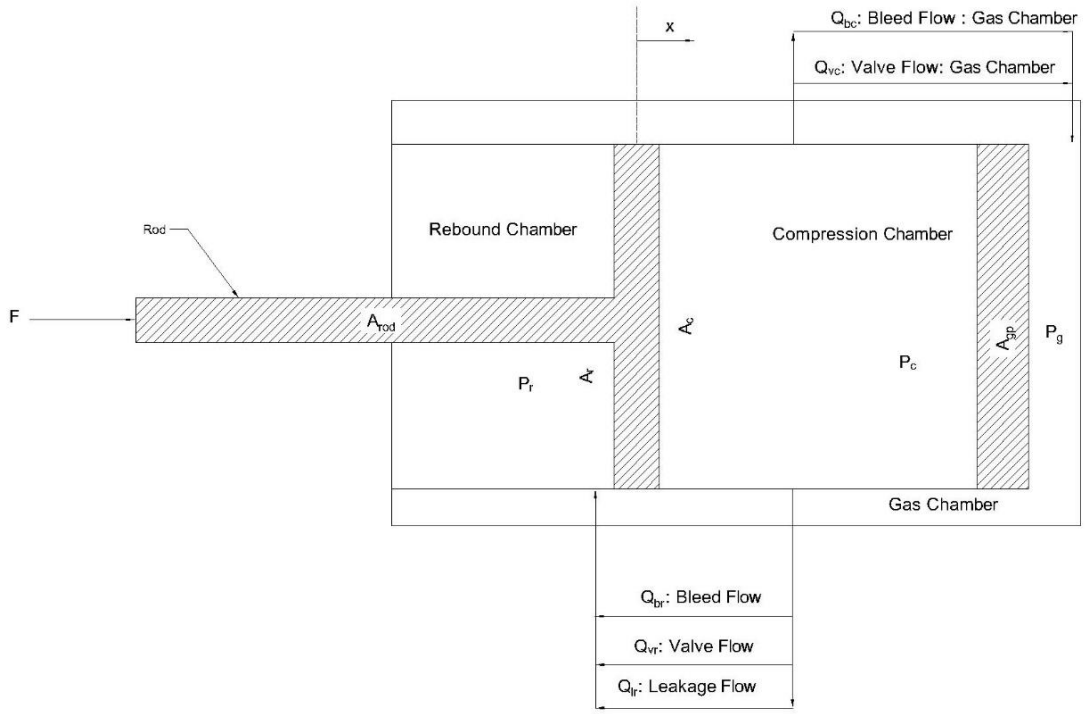

Figure 3-2: Schematic of fluid flow

1. Flow Through Rebound Piston

The flow through the rebound piston is related to the volume of fluid on the rebound side of the piston. To fill or empty the rebound side of the rebound piston flow must pass through the rebound piston and it may occur as valve flow, bleed flow and or leakage flow. So, the total flowrate for a piston moving with a velocity of $\dot{x}$ can be represented as

$$A_r\dot{x} = Q_{vr} + Q_{br} + Q_{lr} \qquad \text{Equation 3.1}$$

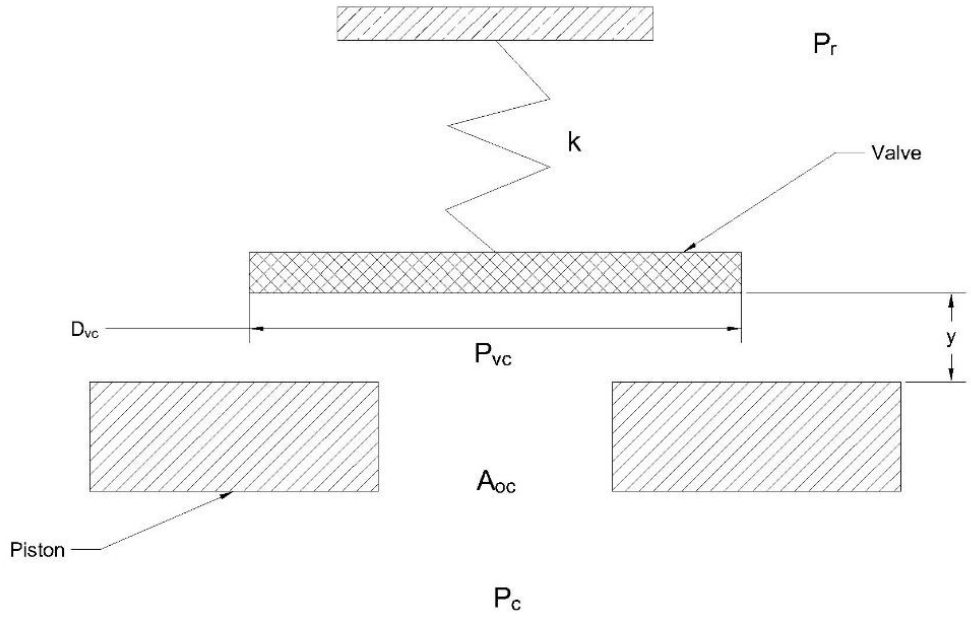

Figure 3-3: Flow through Rebound Piston

a. Flow through Piston Orifice

The pressure loss during flow through rebound piston occurs in two stages. First, the pressure loss occurs as the flow moves from the compression chamber at pressure P_c through the orifice to reach the pressure P_{vr}. Secondly, the pressure loss occurs when the flow is along the shim plate after which the fluid reaches the rebound chamber at pressure P_r. So, the flow is such that the flow rate is constant throughout the valve, Q_{vr}. So, for the flow through the piston orifice the flow rate is:

$$Q_{vr} = C_{Do} A_{or} \sqrt{\frac{2(P_c - P_{vr})}{\rho}} \qquad \text{Equation 3.2}$$

However, Equation 3.2 cannot represent the change in flow that may occur due to the change in viscosity of the fluid. So, to accommodate this change as will be the case of MR fluid during change in magnetic field. So, the flow through piston orifice is represented as the fully developed flow through pipe as:

$$Q = \frac{\pi(P_c - P_{vr})D^4}{128\mu L} \qquad \text{Equation 3.3}$$

b. Flow through Rebound Valve

In accordance with the principle of mass conservation, the flow through the valve is same as the flow through the orifice. However, the pressure difference which causes

the flow in case of valve flow is $P_v - P_r$. Also, the area for the flow is dependent on the deflection (y) and the diameter (D_{vr}) of the shim stack plate. So, the flow through the valve is given by:

$$Q_{vr} = C_{Dv}\alpha\pi D_{vr} y \sqrt{\frac{2(P_{vr} - P_r)}{\rho}} \qquad \text{Equation 3.4}$$

Here, α is the area flow correction factor used to adjust if the whole shim stack does not deflect.

Similar to the flow through piston orifice, to accommodate the change in viscosity, the flow is represented as flow between two parallel plates and is given by Equation 3.5.

$$Q = \frac{\pi y^3 \alpha (P_{vr} - P_r)}{6\mu \ln\left(\frac{r_2}{r_1}\right)} \qquad \text{Equation 3.5}$$

c. Flow through Bleed Orifice

Bleed orifice behaves as a constant opening orifice where flow occurs uninterrupted and due to pressure difference between the compression valve and the rebound valve. Thus, the flow through bleed orifice is:

$$Q_{br} = C_{Db} A_{br} \sqrt{\frac{2(P_c - P_r)}{\rho}} \qquad \text{Equation 3.6}$$

d. Leakage past Rebound Piston

There is small leakage of fluid around the piston due to the pressure difference between compression chamber and rebound chamber i.e. (P_c- P_r). This flow can be modeled by assuming the laminar flow through parallel plates. This assumption is valid and has been presented in (Pritchard, 2011) because the clearance between piston and cylinder, b is very small when compared to the length of the cylinder, l . So, we can apply the Navier-Stokes equations to derive the leakage flow which gives

$$\frac{Q_{lr}}{C_r} = \frac{(P_c - P_r) b^3}{12\mu l}$$

Here, C_r is the circumference of the piston which has been taken as the circumference of leakage. Substituting $C_r = \pi D_p$ into the above equation, we get,

$$Q_{lr} = \frac{(P_c - P_r)\pi D_p b^3}{12\mu l}$$

Leakage also occurs because of the velocity of the piston which is given by:

$$Q_{lr} = \frac{\dot{x} b \pi D_p}{2}$$

By combining the two types of leakage the total flow due to leakage around piston is found to be:

$$Q_{lr} = \frac{(P_c - P_r)\pi D_p b^3}{12\mu l} + \frac{\dot{x} b \pi D_p}{2} \qquad \text{Equation 3.7}$$

The leakage around the piston has been shown schematically in Figure 3-4.

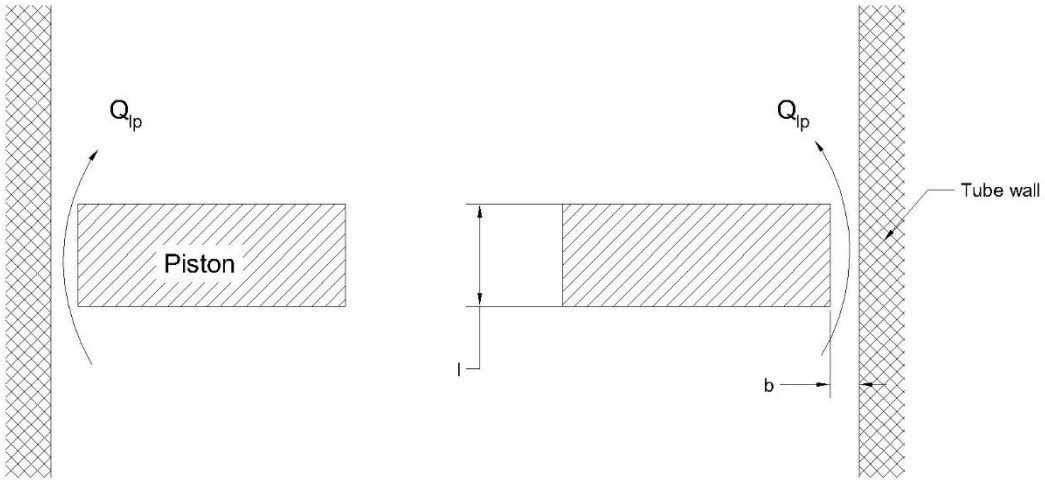

Figure 3-4: Leakage around Piston

2. Flow Through Compression Piston

The flow through Compression Valve occurs in order to accommodate the volume of piston rod. This flow is similar to the flow through the Rebound valve, however the leakage flow is not present. So a volume equal to the volume of the rod needs to flow through this valve either as bleed flow or valve flow, i.e.

$$A_{rod}\dot{x} = Q_{bc} + Q_{vc} \qquad \text{Equation 3.8}$$

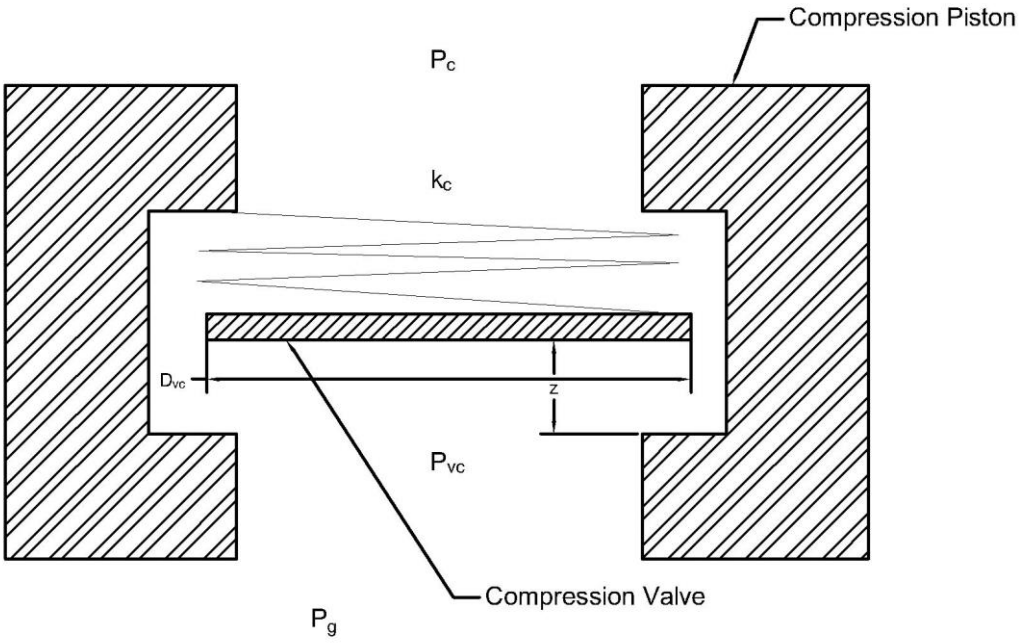

Figure 3-5: Flow through Compression Piston

a. Flow through piston orifice

The flow passes through the orifice provided in the fixed compression piston. This flow is the result of the difference in pressure of compression chamber P_c and the pressure at the valve opening, P_{vc}. P_{vc} is obtained because of the pressure loss in the orifice. So, the flow is a constant area flow dependent on the above mentioned pressure difference and is given by Equation 3.9.

$$Q_{vc} = C_{Do} A_{oc} \sqrt{\frac{2(P_c - P_{vc})}{\rho}} \qquad \text{Equation 3.9}$$

b. Flow through Compression Valve

The flow through the compression valve is a variable area flow dependent on pressure difference between the compression chamber and gas chamber (or reservoir). This pressure difference $(P_g - P_c)$ causes the valve to deflect by a value of z units which provides the area for the flow to occur. The flow can be represented as:

$$Q_{vc} = C_{Dv} \alpha \pi D_{vc} z \sqrt{\frac{2(P_{vc} - P_g)}{\rho}} \qquad \text{Equation 3.10}$$

c. Flow through Bleed orifice

The bleed orifice is fixed orifice provided in between the orifice and the shim stack plates. This flow is independent of the shim-stack opening but depends on the pressure difference on either side of the bleed orifice. The resulting formulation of this type of flow is

$$Q_{bc} = C_{Db} A_{bc} \sqrt{\frac{2(P_c - P_g)}{\rho}} \qquad \text{Equation 3.11}$$

3.2.3. Forces on Components

1. Force on Rebound Piston: During Static Condition

When the damper is in static state as shown in Figure 3-6, there is no valve flow of damper fluid. So, the pressure in the whole damper is uniform. However, the area of the piston on the compression side is greater than the area on the rebound side. So a net force exists due to this difference in area which pushes the piston outwards as shown in Equation 3.12

$$F = P_c A_c - P_r A_r \qquad \text{Equation 3.12}$$

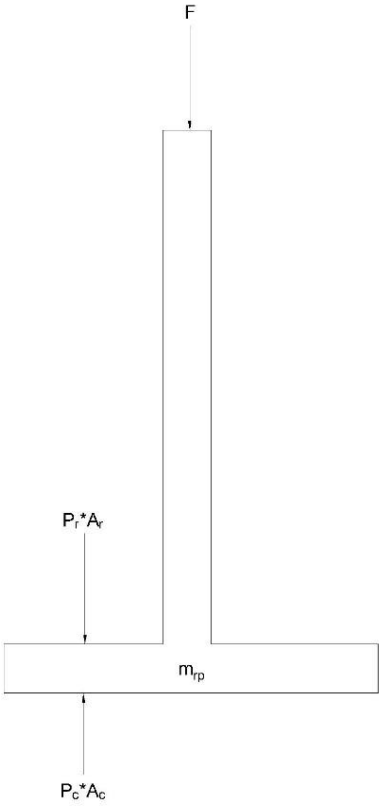

Figure 3-6: Force on Piston during Static Condition

2. Force on Rebound Piston

When the damper is moving, in addition to the static forces as shown in Equation 3.12 the forces as shown in free body diagram of the piston in Figure 3-7 during compression. The force (*F*) on the piston is the damping force generated by the damper. This force is the result of the pressure differences between the compression and rebound side of the piston as well as the friction forces. The friction force presented is the sum of all the friction forces that are present in the system. By summation of forces in the vertical axis, Equation 3.13 is obtained:

$$m\ddot{x} = F - P_c A_c + P_r A_r - F_f \qquad \text{Equation 3.13}$$

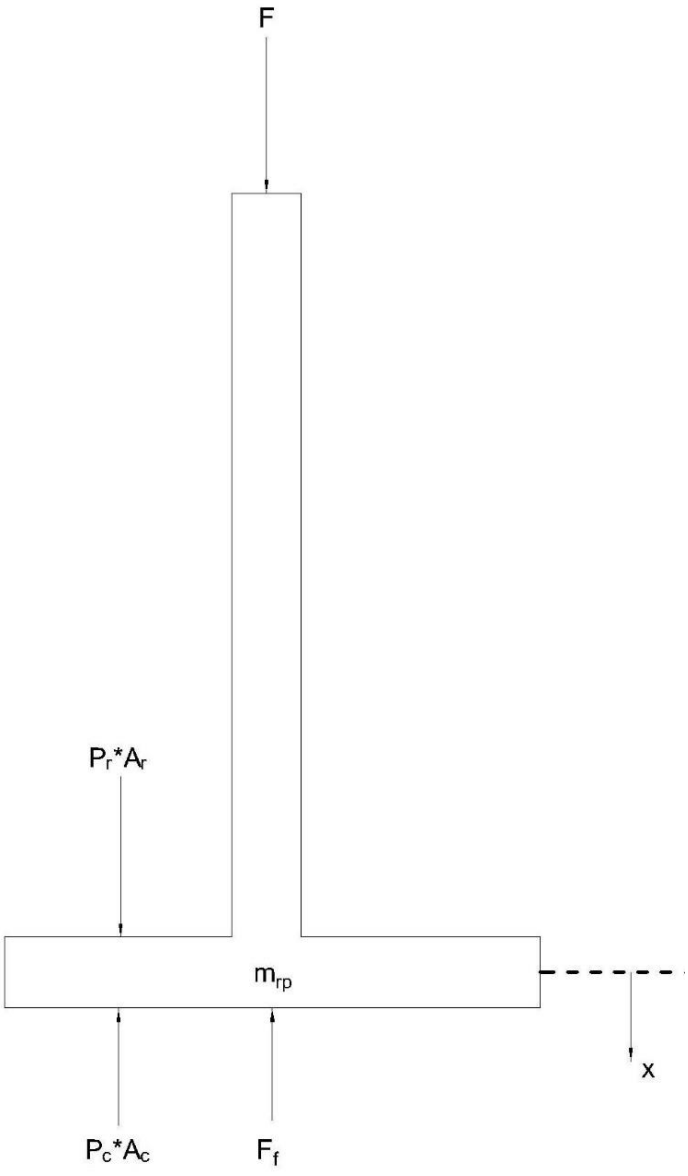

Figure 3-7: Force on the Piston

3. On the Rebound Valve Shim stack

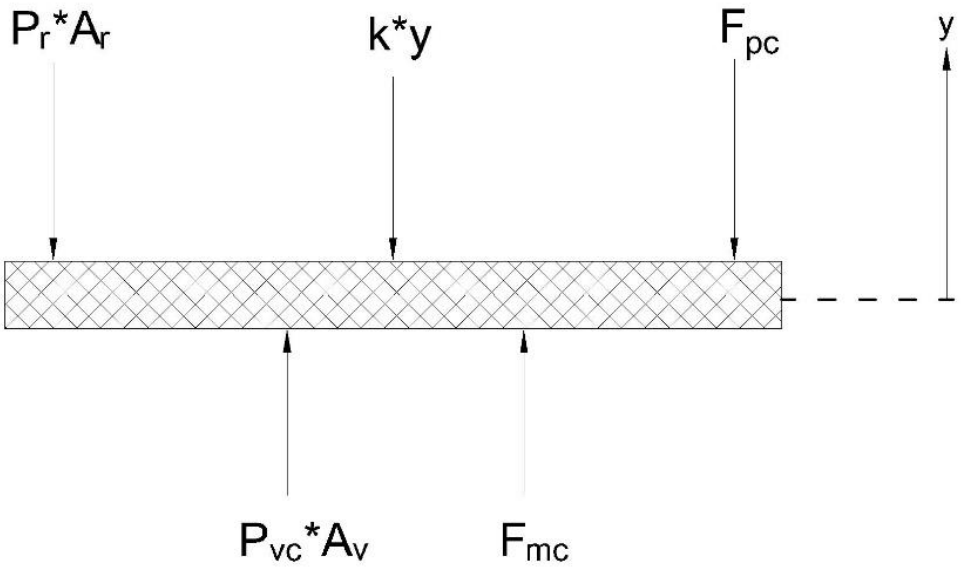

Figure 3-8: Force on Rebound Shim stack

As shown in the free body diagram in Figure 3-8 the forces on the plate can be summed up in the vertical axis to give Equation 3.14. Here, the deflection of the shim plate, *y* can be calculated as

$$k_r y = (P_{vr} - P_r)A_{vr} + F_m - F_{pr} \qquad \text{Equation 3.14}$$

The force due to momentum of the damper fluid, F_m is calculated using the conservation of momentum principle in the vertical axis direction and hence is given by:

$$F_m = \dot{m}_{in} v_{in} - \dot{m}_{out} v_{out}$$

By assuming the flow through the valve is such that the outward flow is perpendicular to the inward flow, the component of v_{out} is zero in the vertical axis direction. Also since,

$$v_{in} = \frac{Q_{vr}}{A_{or}}$$

and,

$$\dot{m}_{in} = Q_{vr}\rho$$

Substituting the values of m_{in} and v_{in} and substituting the value of F_m into Equation 3.15 we get,

$$k_r y = (P_{vr} - P_r)A_{vr} + \frac{\rho C_f Q_{vr}^2}{A_{or}} - F_{pr} \qquad \text{Equation 3.15}$$

Here, C_f is the defined as the momentum force coefficient used to include to effect of flow because the outflow is not perpendicular to the inflow. (Lang & Segel, 1997) have obtained a value of 0.3 for this coefficient through experimental analysis.

4. On the Compression Valve Shim-stack

The compression valve works similar to the rebound valve. So, by applying the same method to find the force balance equation for the compression valve shown in Figure 3-9, we obtain:

$$k_c z = (P_g - P_{vc})A_{vc} + \frac{\rho C_f Q_{vc}^2}{A_{oc}} - F_{pc} \qquad \text{Equation 3.16}$$

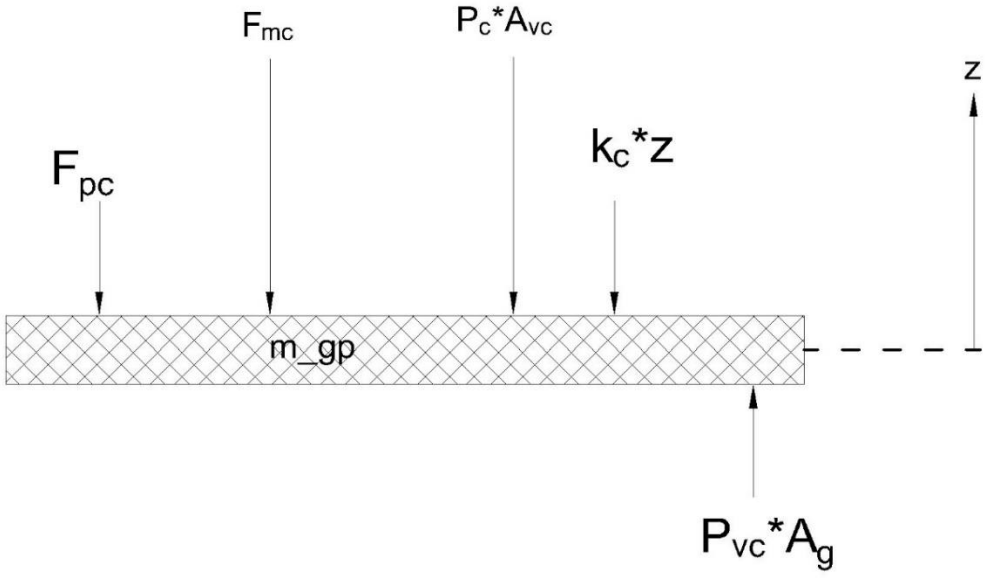

Figure 3-9: Force on Compression Shim stack

3.2.4. Gas Compression

The gas chamber accommodates the volume of the piston rod as it moves inside and outside the cylinder. So, the change of the gas volume is related to the flow through compression piston as described above. The volume of fluid that moves through the compression piston determines the volume change of the gas. Nitrogen gas or other inert gases are normally used so by applying ideal gas law we have,

$$P_1 V_1 = P_2 V_2$$

Here, initial pressure, $P_i = P_{gii}$ is 5 bar and the initial volume, V_i of the chamber is equal to the circumferential area of the chamber in-between the inner and outer tube of the damper times the initial length of the gas in the chamber. So, the gas equation becomes:

$$P_{gi}A_{og}l_i = P_2V_2$$

Also, the final volume of the gas chamber, V_2 is the volume obtained be accommodating the volume of the piston rod in the initial volume i.e. by removing the volume of the rod in case of compression stroke and adding the volume of the rod in the case of rebound stroke. Thus the final volume is

$$V_2 = A_{og}l_i - A_{rod}x$$

Thus the equation of the gas compression is:

$$P_g = \frac{P_{gi}A_{og}l_i}{A_{og}l_i - A_{rod}x} \qquad \text{Equation 3.17}$$

3.2.5. Method of Solution of Mathematical Model of Twin Tube Damper

The model obtained has been solved by using the substitution method of solution of a system of equations. An initial guess was made and by substituting this guess value into relevant equation, a solution was obtained which was substituted into another equation. This was continued until the value for the initially guessed parameter was obtained. If the value obtained in successive iteration was within the convergence criteria, the solution was accepted. This process was repeated for the whole time step, guided by the frequency and amplitude of excitation. This process has been represented for rebound stroke as a flow chart in Figure 3-10.

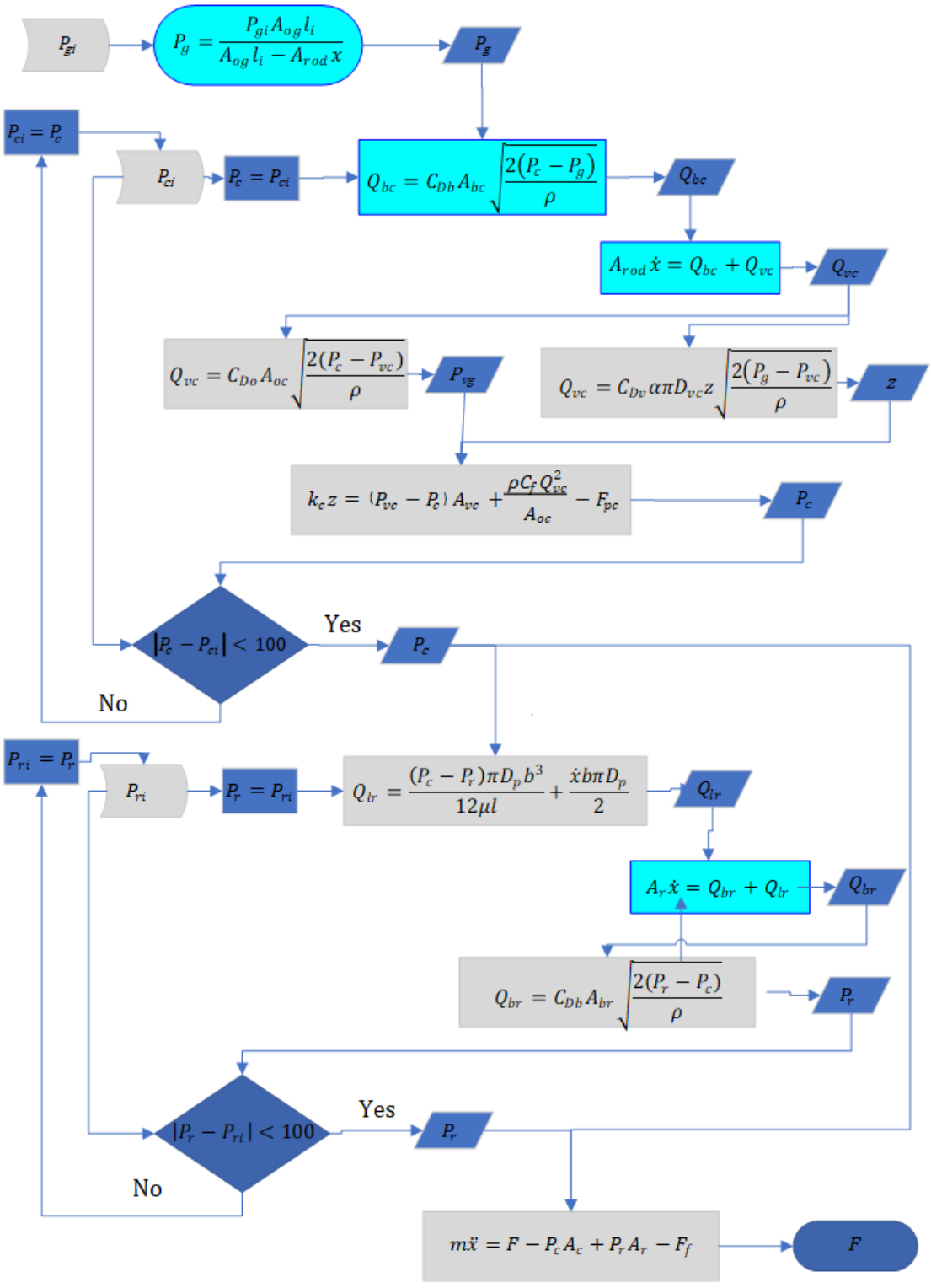

Figure 3-10: Flow Chart of Solution for Rebound Stroke

3.3 Computational Analysis

To validate the mathematical model, results available in literature will be used. In addition, a simplified model of the valve was created and simulated in ANSYS for partial validation. A one-eight model of the damper as shown in Figure 3-11 was created in ANSYS using Design Modeler.

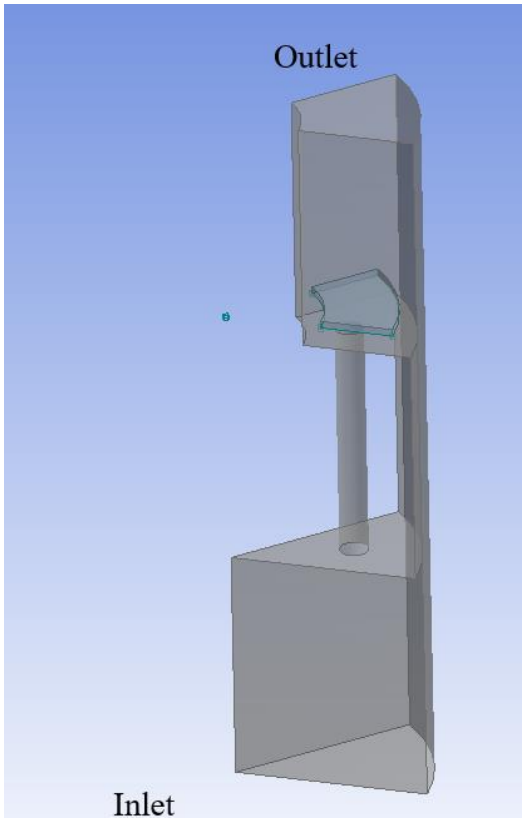

Figure 3-11: Geometry for Computational Analysis

An unstructured mesh was created using ICEM CFD with a maximum size of 0.5 mm and a minimum size of 0.05 mm. First, the mesh was created by defining the part, surface and curve minimum sizes using Robust (Octree) method. Then the volume mesh was deleted and with the remaining surface mesh, the mesh was recalculated using the Quick (Delauney) method. This method is chosen for its speed of computation and the uniformity of the mesh. The mesh was smooth until the quality was above 0.45.

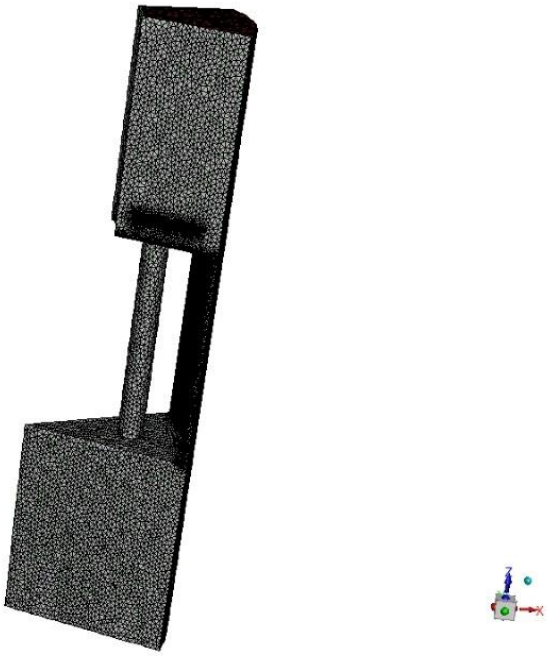

Figure 3-12: Mesh obtained for Computational Analysis

The outputs of the mathematical model were consolidated and those parameters which directly contribute to the Force produced such as Pressure in rebound and compression chamber and deflection of rebound shim stack were used as input for Fluent. Here, the inlet is defined as pressure inlet and the outlet is defined as pressure outlet. Then a laminar flow analysis was done by employing the SIMPLE method of solution. The analysis was done for 3000 iterations with a convergence criteria of 1e-5 for continuity, x-, y- and z- velocity. The methodology is represented as a flow chart in Figure 3-13.

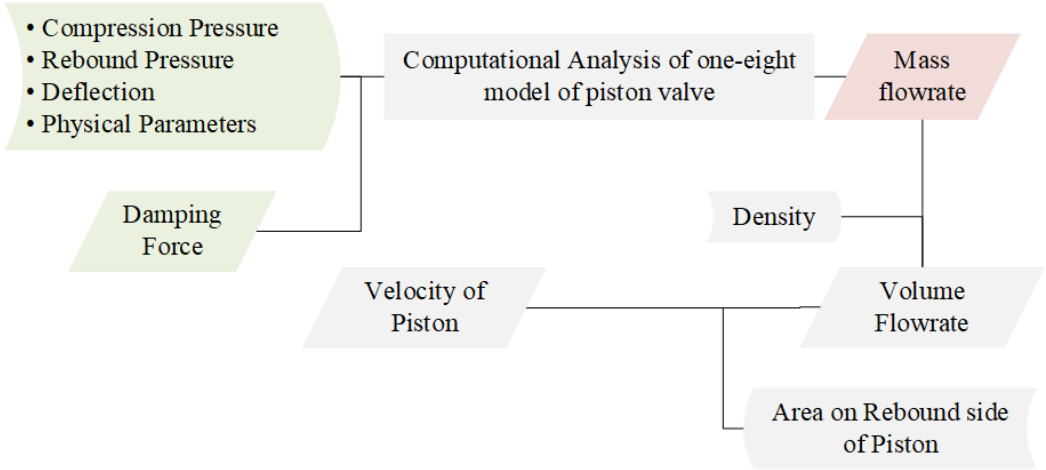

Figure 3-13: Flowchart of Computational Analysis

3.4 Magnetic Analysis

MR dampers employ MR fluids whose inherent properties can be altered to accommodate the change in road excitation and hence increase the range of road excitation for which the damper can perform its work satisfactorily. So, it is important to find how the properties of MR fluid change with the application of magnetic field. So, an analytical analysis was done to determine the magnetic field which will be induced in the fluid and then according to the induced field, the viscosity of the fluid can be determined. So, to simplify the calculation the CAD model has been simplified as shown below:

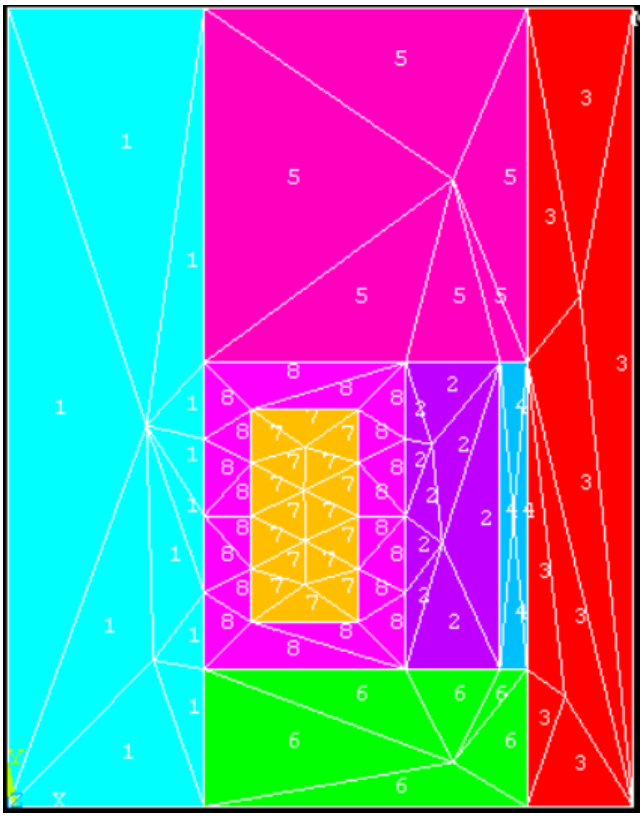

Figure 3-14: Model for Axisymmetric Analysis of Magnetic Flux Density

In the Figure 3-14, the numbering is according to the material type. Here,

Table 3.2: Material Properties for Magnetic Analysis

Material Number	Component	Material Type	Material Property
1,3,4	Piston Rod	Steel	$\mu_r = 75$

<table>
<tr><td>2,5,6</td><td>Fluid Gap</td><td>MR Fluid</td><td><table><tr><td>H</td><td>B</td></tr><tr><td>200</td><td>0.75</td></tr><tr><td>300</td><td>1</td></tr><tr><td>500</td><td>1.25</td></tr><tr><td>600</td><td>1.8</td></tr></table></td></tr>
<tr><td>7</td><td>Coil</td><td>Copper</td><td>$\mu_r = 1$</td></tr>
<tr><td>8</td><td>Air Gap</td><td>Air</td><td>$\mu_r = 0.005$</td></tr>
</table>

With the parameters tabulated above the magnetic analysis was first carried out analytically,

By theory, in parallel magnetic paths,

$$mmf_{path\ 1} = mmf_{path\ 2} = mmf_{path\ 3} = \ ...$$

And in series magnetic paths,

$$total\ mmf\ = \sum_{i=1}^{n} mmf_{path\ i}$$

Thus, $mmf_{MR}\ =\ mmf_{air}\ =\ mmf_{piston}$

$$\frac{\phi_{MR} * L_{MR}}{\mu_{MR} * A_{MR}} = \frac{\phi_{air} * L_{air}}{\mu_{air} * A_{air}} = \frac{\phi_{piston} * L_{piston}}{\mu_{steel} * A_{piston}}$$

And

$$mmf_{piston\ rod}\ =\ mmf_{upper\ air\ gap}\ =\ mmf_{lower\ air\ gap}$$
$$=\ mmf_{MR}\ +\ mmf_{air}\ +\ mmf_{piston}$$

Also, $B_i = \frac{\phi_i}{A_i}$

And $Ampere - turns_i = \frac{B_i * L_i}{\mu}$

$$Total\ Ampere - turns = \sum_{i=1}^{n} Ampere - turns_i$$

But, $Total\ Ampere - turns = Number\ of\ turns * Current$

These equations can be solved for different values of current flowing through a coil with standard number of turns. The solution results in values of magnetic flux density induced at the MR fluid region. The final equation for the magnetic flux density induced in the MR fluid region in terms of current (I) flowing through (N) turns of coil is:

$$B_{MR\ fluid} = \frac{\phi_{MR\ fluid}}{A_{MR\ fluid}} = \frac{N * I}{1.45 * 10^{8} * A_{MR\ fluid}}$$

Where, $A_{MR\ fluid}$: $Cross\ sectional\ area\ of\ MR\ fluid\ gap\ in\ sq.m = 118.5 * 10^{-6}$

$$\therefore B_{MR\ fluid} = \frac{N * I}{17182.5} \qquad \text{Equation 3.18}$$

Here,

$$Number\ of\ Turns, N = \frac{Area\ of\ Coil\ Region}{Area\ of\ one\ coil}$$

From geometry, Area of Coil Region= 0.000012465 m^2

For AWG 24-gauge copper wire, diameter, d= 0.51054 mm

Area of one coil= $2.047 * 10^{-7}$

Thus, Number of turns, $N = 61.10294 \cong 62$ turns

To verify the accuracy of the analytical solution, the magnetic analysis was carried out in ANSYS employing a 2D axisymmetric approach.

The features of the analysis were as follows:

Element Type: Plane13

It has 2D magnetic, thermal, electrical and piezoelectric field capability with a capability of modeling B-H curves.

Boundary Condition: Flux Parallel Solution

Global Element Size: 0.025 m

Convergence Criteria: 0.001

Steps:

1. The CAD model was simpified to reduce computational complexity.

2. Physical attributes were assigned to each part and different regions of the model by meshing the model.
3. Boundary conditions were provided and excitations in the form of current density was applied.
4. The model was solved for Magnetic flux induced.

Assumptions:

The flux doesnot leak out of the system.

• The element must lie in a global X-Y plane

• Y-axis is the axis of symmetry for axisymmetric analysis

CHAPTER FOUR: RESULTS AND DISCUSSIONS

4.1 Pressure

The pressure of the fluid plays an important role in the amount of damping force produced by the damper. It is directly related to the damping force as shown in Equation 3.13. So, if a higher pressure difference can be obtained across the piston, the higher the damping force can be. The major pressure zones to be considered for proper analysis of the damper are:

1. Rebound Pressure

The variation of the rebound pressure is as shown in Figure 4-1.

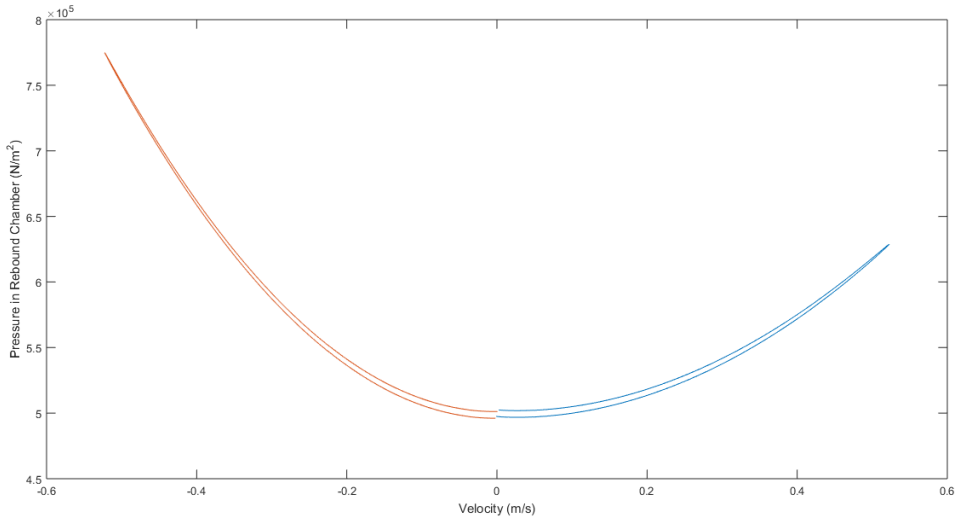

Figure 4-1: Variation of Rebound Chamber Pressure with Velocity

It is the pressure of fluid in the rebound chamber. The excitation is provided when the damper piston is at the middle of the damper such that the amplitude of oscillation is contained within the damper. When the piston is at the bottom of the cylinder, the pressure of the rebound chamber is at a value slightly lesser 5 bar. This is because of the momentum of the piston which is pushing it further downwards. Then the piston starts accelerating and reverses in direction which causes the increase in pressure of rebound chamber until it reaches the middle of the stroke where the maximum pressure of 7.7 bar is obtained in the rebound chamber. Once at the middle of the stroke, the piston starts to decelerate and rebound pressure decreases. When the piston reaches the top, the momentum of the piston causes the pressure to be slightly higher than 5 bar. Then it changes direction once more and begins to accelerate towards the middle of the

stroke. During this motion, the volume of the rebound chamber goes on increasing but the incoming fluid from the high pressure compression chamber controls the pressure in the chamber. So, the rebound pressure increases by a small amount to 6.2 bar. When it reaches the middle of the stroke it again starts decelerating and the rate of increase of pressure in the compression chamber begins decreasing. Consequently, the pressure in the rebound chamber also drops and reaches 4.9 bar and the cycle is repeated.

2. Compression Pressure

The compression pressure changes in the opposite manner to the rebound pressure. When the piston is at the bottom of the stroke, the compression chamber pressure is minimum at around 5 bar. As the piston moves upward and until it reaches the middle of the stroke, the piston accelerates. During this motion, the volume of the compression chamber increases which tends to decrease the pressure but the pressure is maintained at around 5 bar by the inflow of fluid from the high pressure gas chamber. When the piston reaches the middle of the stroke, the piston continues its motion upwards but the motion is decelerated. So, the pressure in the chamber increases slightly due to the effect inflow of liquid from the gas chamber which is still at a higher pressure than the compression chamber. Once at the top of the stroke, the piston reverses direction and starts to accelerate again which causes the rapid increase in the pressure of the compression chamber. This increase in pressure continues till the piston continues accelerating and reaches the middle of the stroke. The highest pressure in the compression chamber is reached during this motion which is nearly equal to 9 bar. When the piston reaches the mid-stroke position, the piston begins to decelerate. This deceleration causes the pressure to drop as its pressure is required to push fluid into both rebound chamber and reservoir (gas) chamber both of which are at a high pressure themselves. This variation is as shown in Figure 4-2.

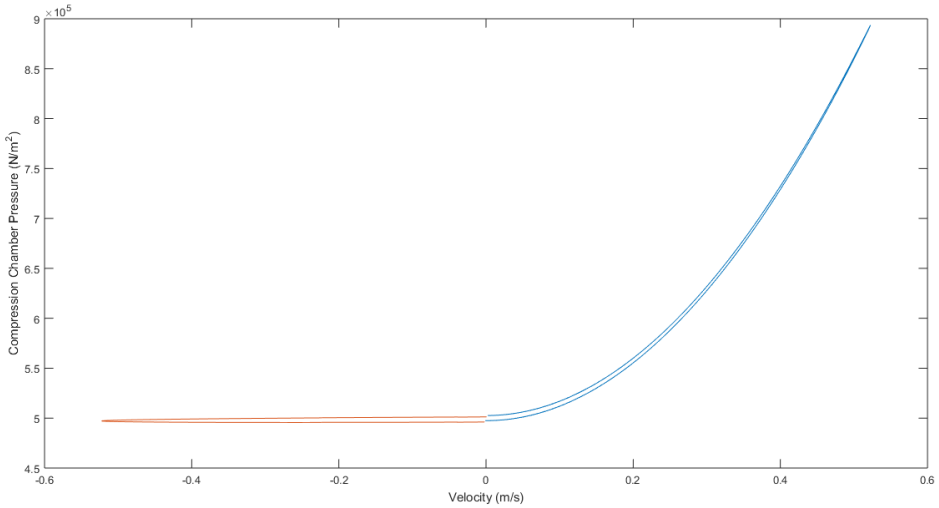

Figure 4-2: Variation of Compression Chamber Pressure with Velocity

3. Comparison:

The plot for Pressure v/s velocity is an important aspect of damper modeling. In a similar study by (Meissen, 2009) he has presented the variation of pressure which is as shown in Figure 4-3.

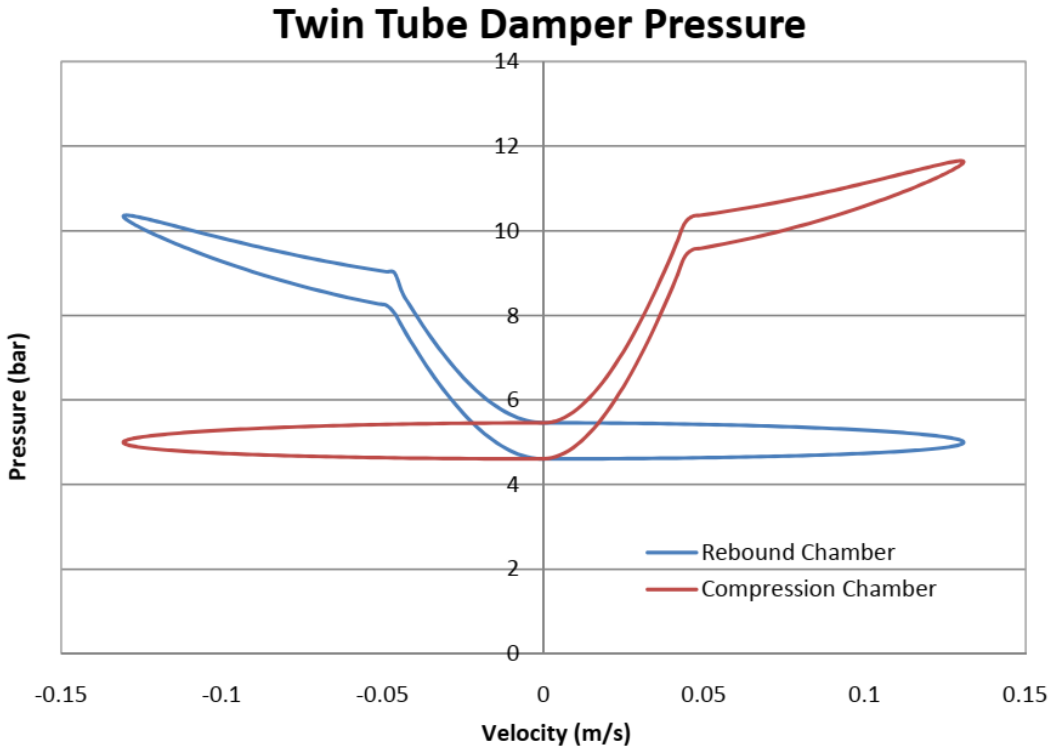

Figure 4-3: Variation of Pressure with Velocity

(Source: (Meissen, 2009))

Although, the analysis methods and parameters of the damper were different, this is similar to the results obtained through this study as shown in Figure 4-4 which has been obtained by combining the pressure in rebound and compression chambers.

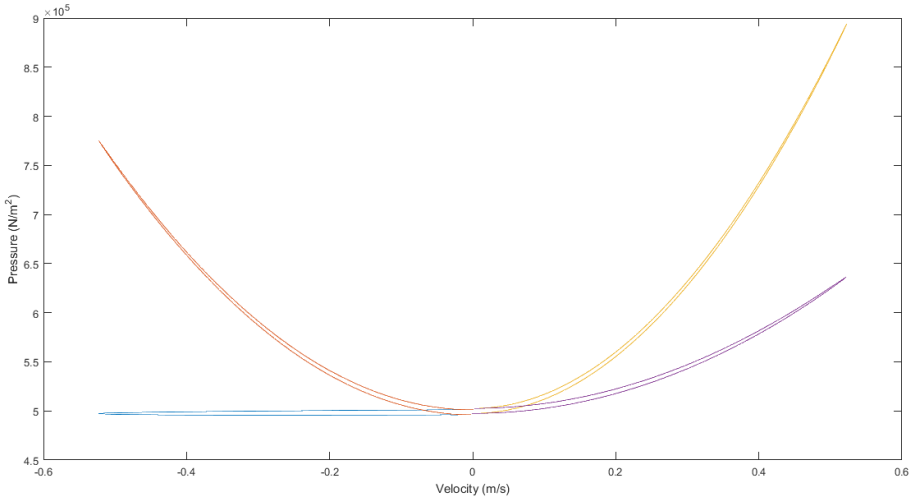

Figure 4-4: Variation of Pressure with Velocity

The major difference in the graphs are the settling of the pressure at around the highest value. This can be attributed to the difference in the types of dampers used for modeling. While this study focused on the conventional damper, (Meissen, 2009) had used a damper which possessed external valves connecting the rebound, compression and gas chambers which enables the settling of the pressure.

4.2 Force

The damping force that the damper provides is a function of velocity. It can be presented in different ways but the most common method to depict the relation is the continuous velocity plot (CVP). The CVP has been created and is shown in Figure 4-5. In the figure, we can see than the maximum force attainable through the use of the damper is around 175N in the compression stroke and 100N in the rebound stroke when the model is tested at 3.2 Hz and amplitude of 26 mm. At 0m/s velocity i.e. when the piston is at the end of the stroke either at the top or bottom, the force produces is nearly negligible. A small amount exists which is caused due to the hysteresis of the damper. As the damper begins to move from the bottom of the stroke, the damper accelerates, and the fluid is forced through the bleed valves in the rebound piston into the compression chamber. So, a force which opposes this motion of the piston is generated which is

increasing until the middle of the stroke is reached. Once , the piston reaches the middle, it continues its motion towards the top of the stroke, however, the motion is decelerated. So, the damper still produces a force which opposes the upward motion of the piston but the force gets gradually lessened as the piston moves up, because the piston is itself decelerating. When the piston reaches the top of the stroke, it produces a negligible amount of force. Then, it reverses its direction and then starts to accelerate in the compression stroke. At the beginning of the stroke, the force produced by the damper has to oppose the accelerating motion of the damper, so the force also goes on increasing. It reaches the maximum force of 175N when the piston reaches the middle of the stroke after which the piston continues the compression stroke but in a decelerating manner. This decelerating motion of the piston means that the force produced by the damper to oppose it gradually decreases until it reaches the bottom of the stroke.

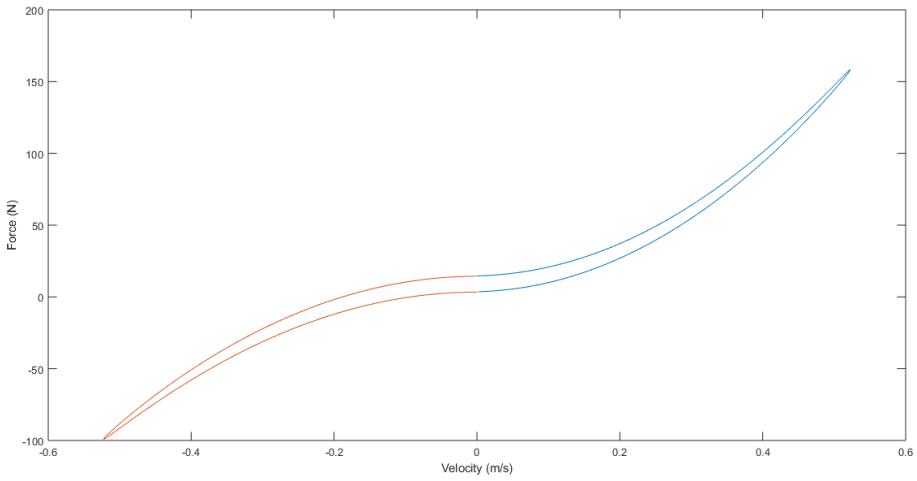

Figure 4-5: Variation of Force with Velocity

In the figure above, the force generated by the damper is asymmetrical about the horizontal axis. This is because the fluid has to pass through different types of restrictions during the course of rebound stroke and compression stroke.

The variation in force with velocity for excitation of amplitude 15 mm and different frequencies is shown below:

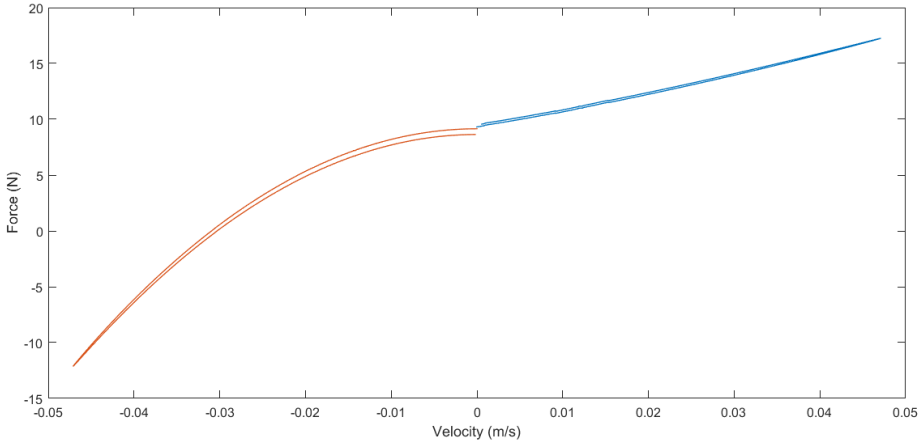

Figure 4-6: Force vs velocity for 0.5 Hz

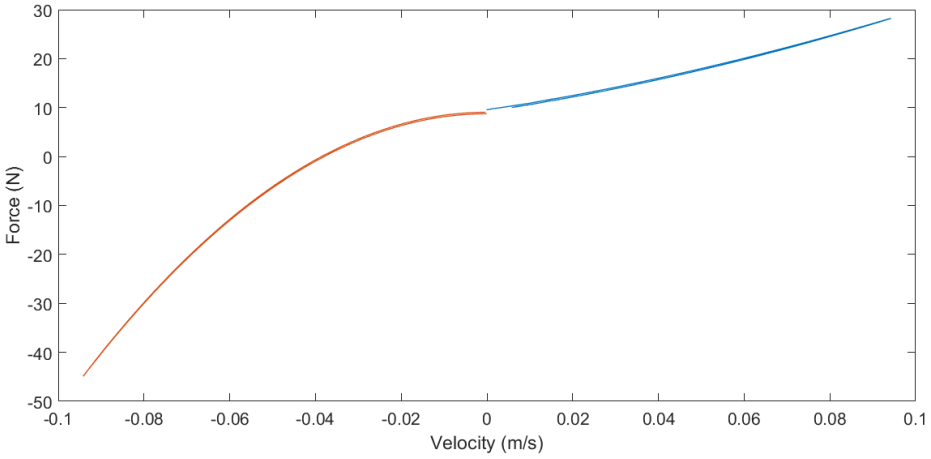

Figure 4-7: Force vs velocity for 1 Hz

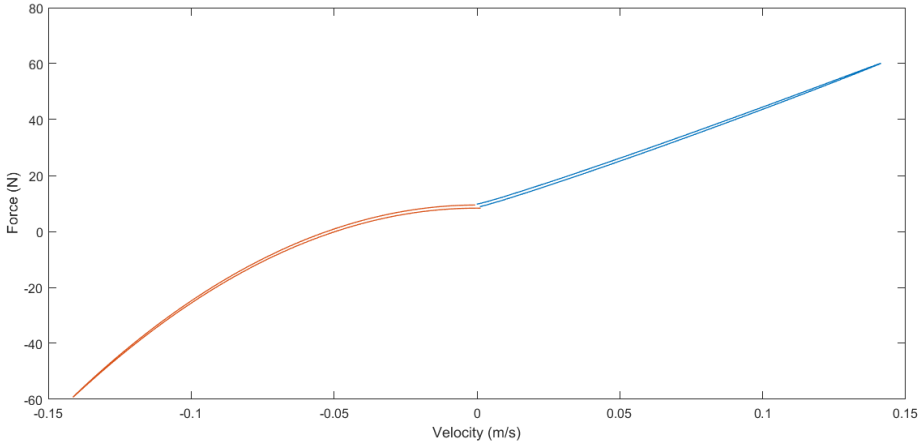

Figure 4-8: Force vs velocity for 1.5 Hz

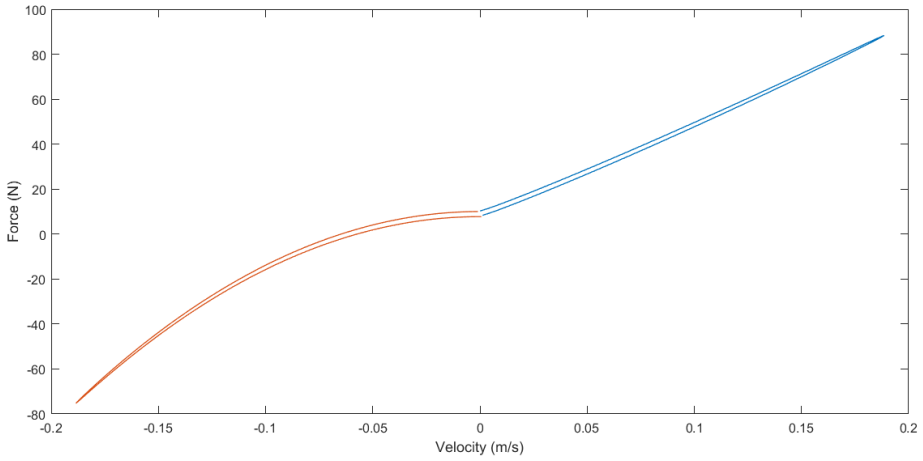

Figure 4-9: Force vs velocity for 2 Hz

(Barethiye, Pohit, & Mitra, 2017) had conducted experimental study and found the CVP as shown in Figure 4-10. It can be seen that by changing the excitation frequency, the magnitude of the force gets changed but the pattern of the variation remains the same. This pattern is similar as observed in the CVP obtained as the result of the mathematical modeling of this study. The magnitude of force is dependent on the physical parameters of the damper eh

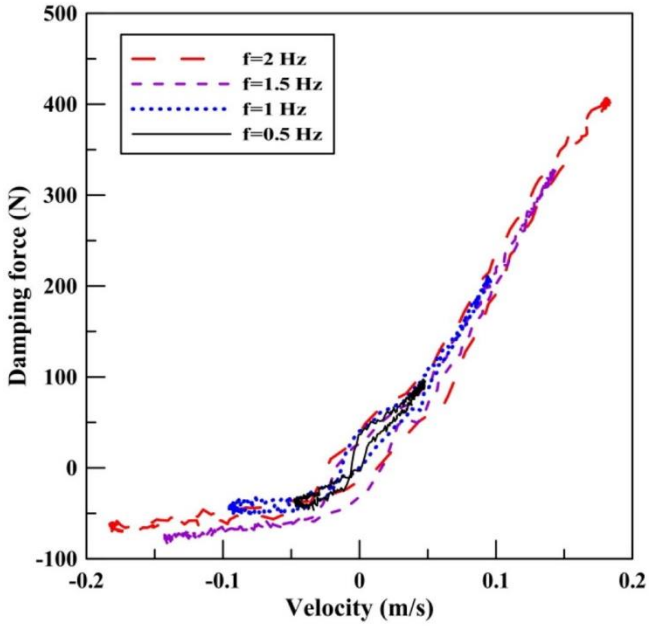

Figure 4-10: Variation of Force with Velocity

(Source: (Barethiye, Pohit, & Mitra, 2017))

Another way of representing the force produced by the damper is to plot the force against the displacement of the piston as shown in Figure 4-11.

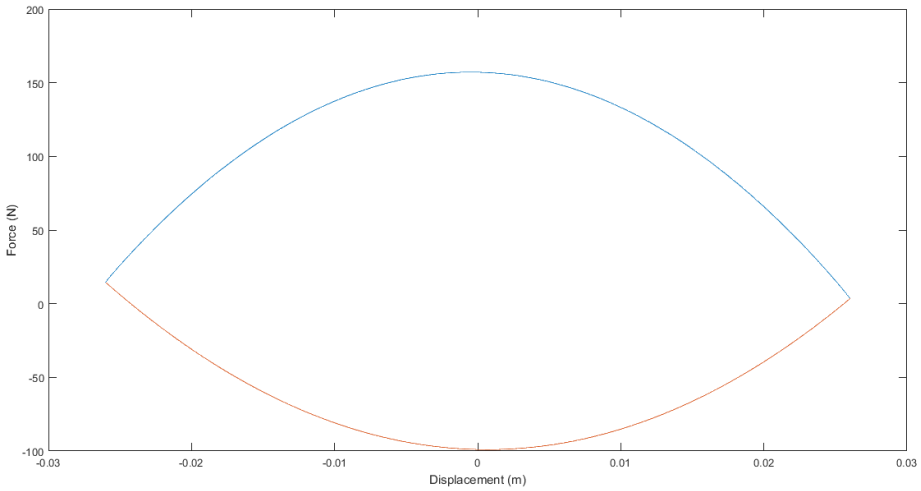

Figure 4-11: Variation of Force with Displacement of the piston

4.3 Results of Computational Analysis

The one eight model was simulated. The simulation provided the mass flow rate through the outlet, which was used to mathematically calculate the volume flowrate and then by using Equation 3.1 the velocity of the piston was calculated as shown in table

Table 4.1: Comparison of Analytical and Computation Velocity for Force Variation

Force (N)	Analytical Velocity (m/s)	Computational Velocity (m/s)
17.3	0.02	0.020232
24.9	0.04	0.042989
32.96	0.06	0.051318
41.11	0.08	0.06717
49.68	0.1	0.080604
58.24	0.12	0.092963
66.89	0.14	0.112845
84.69	0.18	0.151857

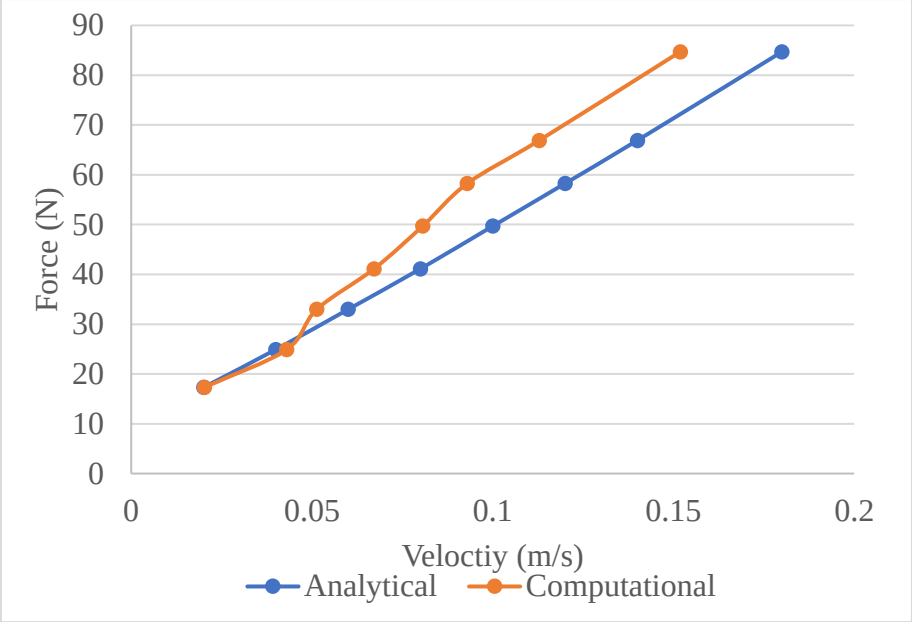

Figure 4-12: Comparison of Analytical and Computation Velocity for Force Variation

Figure 4-12 shows the trend of the Force- velocity relation for analytical and computation methods. The computational method initially shows a larger velocity when the same force is applied. As the force gets larger however, the velocity is smaller for the same force. This may be because at higher force, the velocity is restricted by the wall which is present in the one-eight model to define the domain. If the simulation was run with the full model of the damper, the model will not have the wall that divide the damper into 8 parts and hence resemble the mathematical model more precisely.

4.4 Solution of Magnetic Analysis

The magnetic analysis was conducted in ANSYS and the simulation was run such that the flux is contained within the damper walls. The analysis is done by supplying the model with discrete input current of 0.1875A, 0.25A, 0.375A, 0.5625A and 3A. These values of current have been chosen as could be found in literature. The analysis provided the values of magnetic field induced in the orifice region of the damper. Since, MR fluid passes through the orifice, the magnetic field gets induced in the fluid and its properties gets altered. The viscosity of the fluid gets changed with the change in magnetic field induced in the MR fluid.

The ANSYS analysis results in the magnetic field density that is distributed across the region. The results of the ANSYS analysis are given below and for comparison with the analytical results the average of the Magnetic field induced in the region is averaged over the region.

For I=0.1875 A

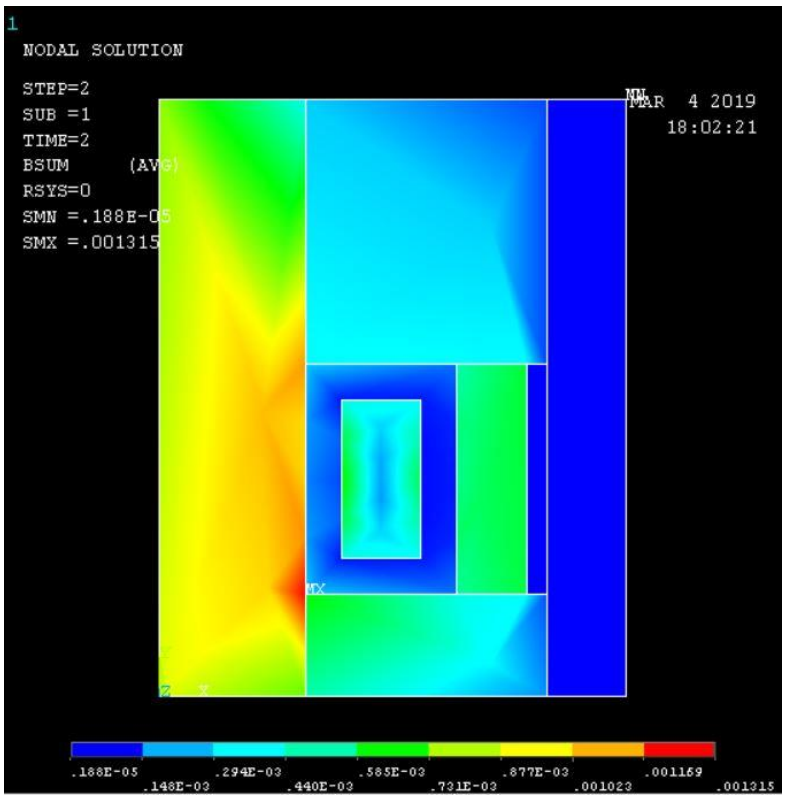

For I=0.25 A

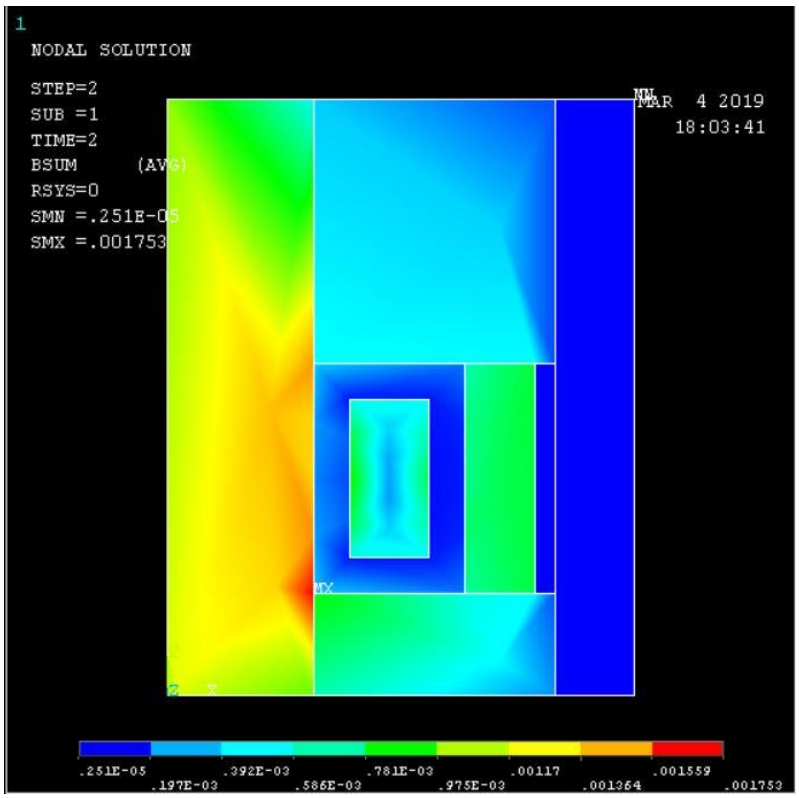

For I= 0.375 A

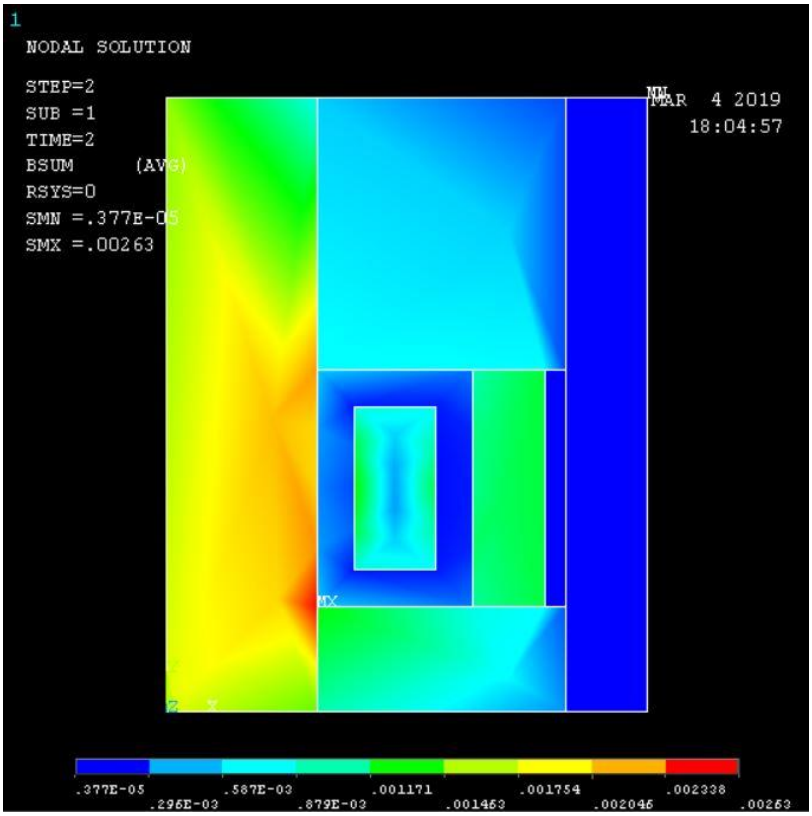

For I= 0.5625A

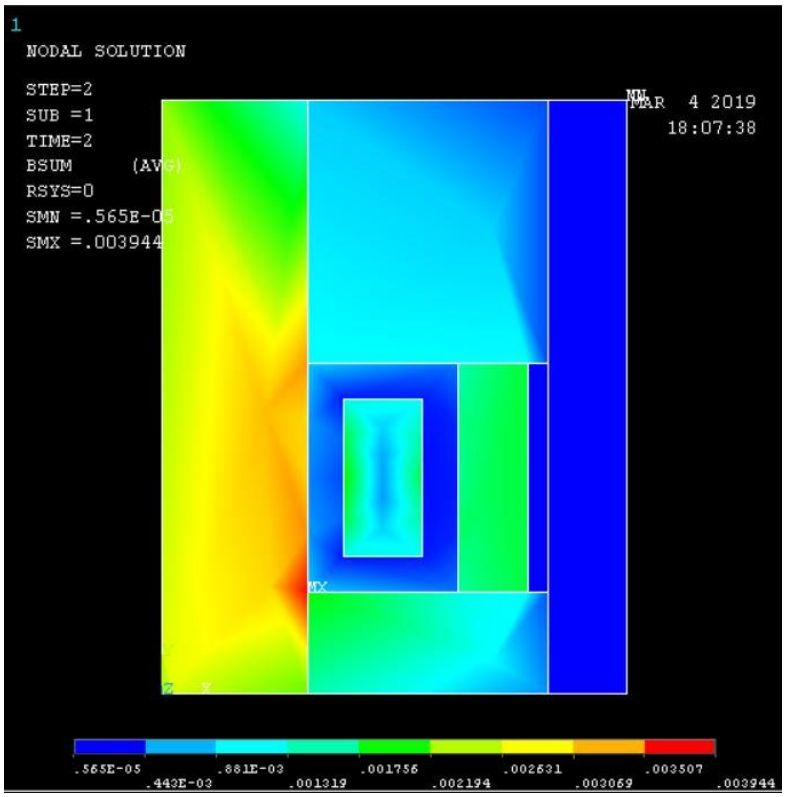

For I= 3 A

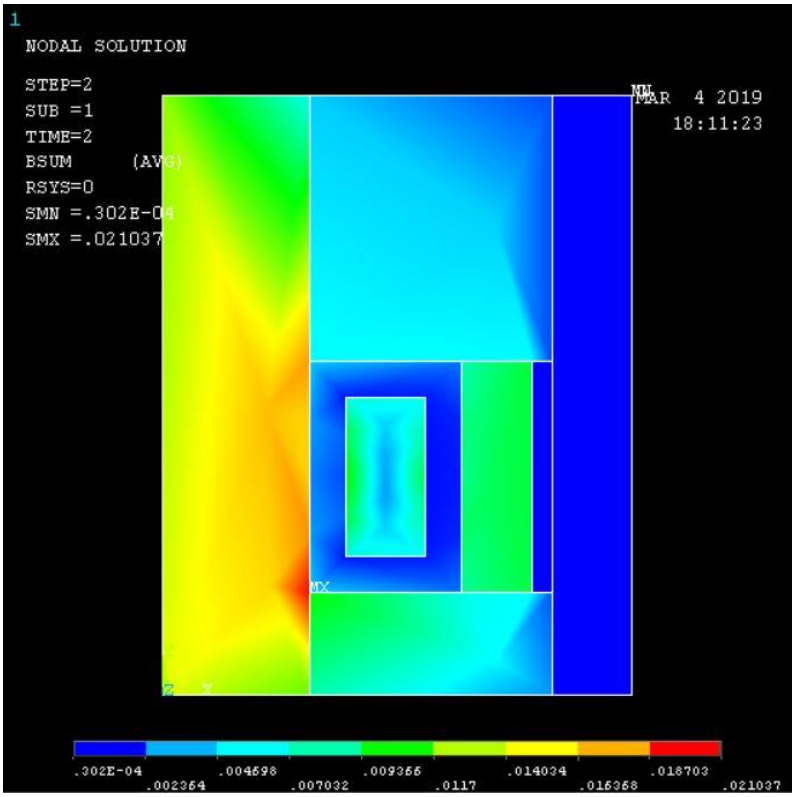

Figure 4-13: Results of Magnetic Analysis

The results from the analytical analysis and computational analysis show that the magnetic field induced increases with the current applied to the coil. The comparison between the analytical results and results from simulation is given in Table 4.2 and Figure 4-14.

Table 4.2: Summary of Magnetic Analysis

Current (I)	Current Density (J)	Analytical Result (T)	Ansys Result (T)
0.1875	932611.3117	0.00067656	0.000804
0.25	1243481.749	0.00090208	0.0010725
0.375	1865222.623	0.00135312	0.0016035
0.5625	2797833.935	0.00202968	0.0023625
3	14921780.99	0.01082497	0.012867

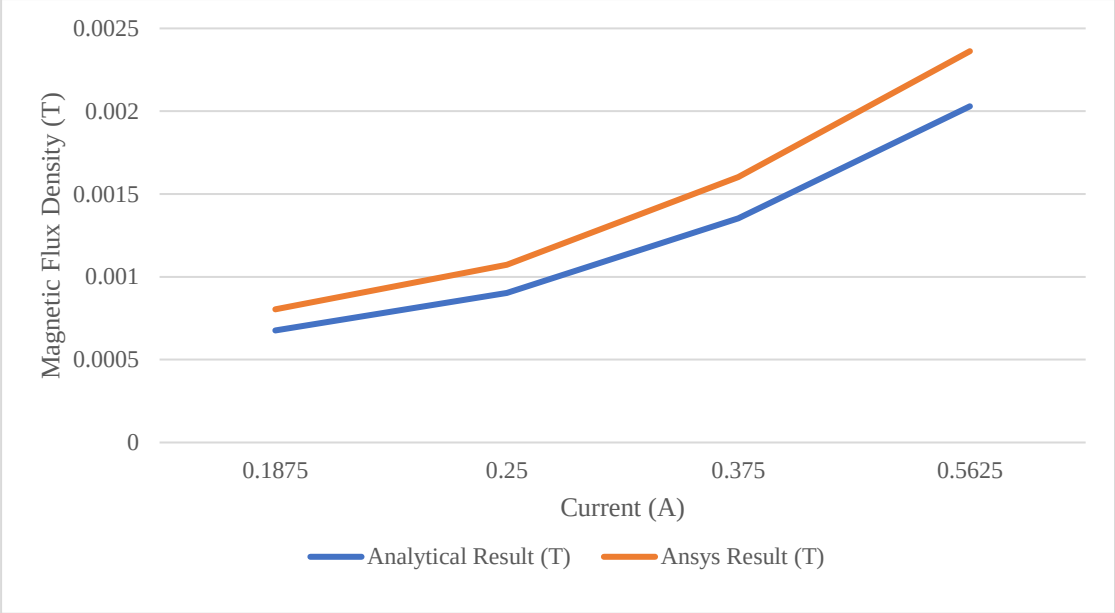

Figure 4-14: Variation in Magnetic Flux Density due to applied current

By using the graphically available dependence of the viscosity on the magnetic induction, we can summarize the following values of viscosity for further analysis:

Table 4.3: Viscosity of MR fluid for applied current

Current (I)	Viscosity (Pa.s)
0.25	0.2
0.375	0.22
0.5625	0.4

4.5 Force for MR damper

Finally, the force response variation with velocity for a MR damper is obtained by altering the viscosity of the model.

Force obtained through the damper is changed when the magnetic field is applied to it. The force is dependent on the apparent viscosity of the fluid which is dependent on the magnetic field. With the relation of viscosity with magnetic field, the viscosity of the fluid was obtained and applied to the mathematical model. The change hence obtained is shown as:

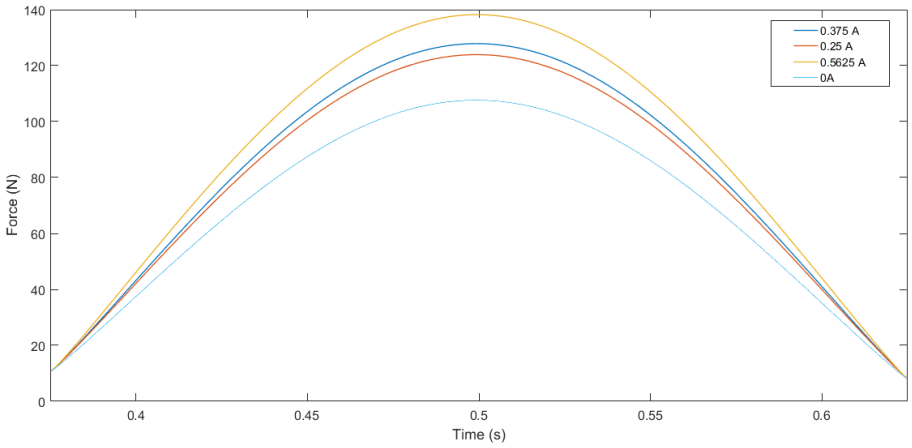

Figure 4-15: Force vs time

The damping force obtained increases with the increasing viscosity and increasing current. The model was run for 2 Hz frequency and amplitude 20 mm in the compression stroke. For this configuration, the maximum force of about 138 N was achieved when a current of 0.56 A was applied to the coil, at which point the magnetic field induced is 0.002 and the apparent viscosity is 0.4 Pa.s. This is a 29% greater than the force obtained at 0 A. This indicates that the force can be controlled over a wide range with a small current excitation.

(Ashfak, Saheed, Rasheed, & Jaleel, 2009) had conducted an experiment to determine the variation of force with time which has resulted in:

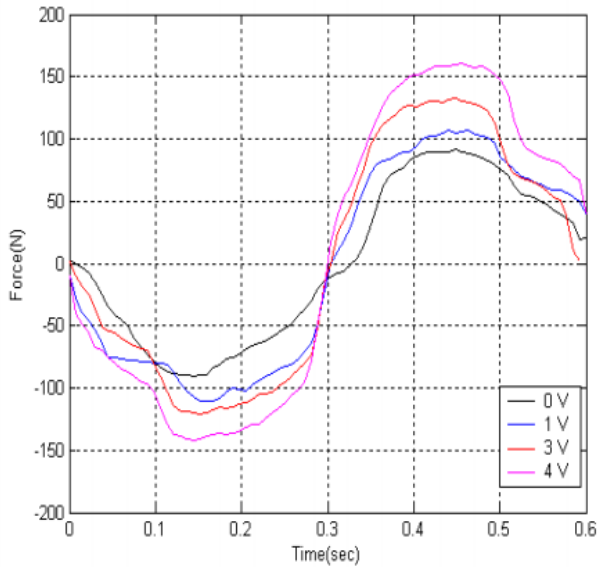

Figure 4-16: Variation of Force with Time

(Source: (Ashfak et al., 2009))

It can be seen in Figure 4-16, that the increase in current applied to the damper causes the damper to produce more damping force. In the compression region there is an increase of 77% in the damping force for an increase in voltage of 4 V. The difference is very large compared to the results from the mathematical model. However, the mathematical model was subjected to an increase of 0.04 V due to the limitation in data available for the viscosity in literature.

CHAPTER FIVE: CONCLUSIONS AND RECOMMENDATIONS

5.1 Conclusions

The mathematical model created in this study predicts the nonlinear asymmetric behavior of the damper. The results show that the force increases with increasing velocity when other factors are constant. Force also increases with the increasing frequency of excitation and the increase in amplitude of excitation.

The damper model was then subjected to magnetic analysis by changing the conventional damper fluid to a MR damper fluid. The magnetic field induced in the fluid increases with the increase in the current flowing in the coil. This result was further used to calculate the apparent viscosity of the damper fluid at the excitation current. The viscosity of the fluid reached 0.4 Pa.s for 0.5 A of current in contrast to 0.11 Pa.s at no excitation current.

The model hence created facilitates the changing of properties of the damping fluid. This was achieved through a provision of explicitly defining the dynamic viscosity coefficient of the damper fluid in the model. When the value of apparent viscosity due to the current was input into this model, the force obtained due the application of magnetic field was calculated. The results show an increase of 29% in the damping force produced for an increase of 0.5 A of current.

5.2 Recommendations

Further work may include the effect of compressibility and temperature on the properties of the damper fluid which will result in accurate prediction of the hysteresis observed in the experimental models.

Further research is necessary to understand the behavior of MR fluid at higher current excitation and magnetic field. Further testing and validation of other dampers would also be beneficial. This would further validate the accuracy of the model and would allow comparison between design differences between dampers.

REFERENCES

1) Ashfak, A., Rasheed, K. K., & Jaleel, J. A. (2013). Modeling, Simulation and Experimental Validation of Magneto-Rheological Damper. *International Conference on Advanced Nanomaterials & Emerging Engineering Technologies* (pp. 267-274). Chennai: Sathyabama University.

2) Ashfak, A., Saheed, A., Rasheed, K. K., & Jaleel, J. A. (2009). Design, Fabrication and Evaluation of MR Damper. *International Journal of Mechanical and Mechatronics Engineering*, 530-535.

3) Barethiye, V., Pohit, G., & Mitra, A. (2017). A combined nonlinear and hysteresis model of shock absorber for quarter car simulation on the basis of experimental data. *Engineering Science and Technology, an Internation Journal*.

4) Dixon, J. D. (2007). *The Shock Absorber Handbook.* Sussex: John Wiley & Sons Ltd.

5) Guglielmino, E., Sireteanu, T., Stammers, C. W., Ghita, G., & Giuclea, M. (2008). *Semi-active Suspension Control.* London: Springer.

6) K., H., A., G., Kumar, H., & Gangadharan, K. V. (2014). Analysis of MR damper based on Finite Element Approach.

7) Kashem, S., Nagarajah, R., & Ektasabi, M. (2018). *Vehicle Suspension Systems and Electromagnetic Dampers.* Singapore: Springer.

8) Lang, H. H., & Segel, L. (1997). *A Study of Characteristics of Automotive Hydraulic Dampers at High Stroking Frequencies.* Arbor: Ph.D Dissertations The University of Michigan.

9) Meissen, C. R. (2009). *Development and Validation of a Physical Model for a Damper.* Colorado: Colorado State University.

10) Mihai, I., & Andronic, F. (2014). *Behavior of a semi-active suspension system versus a passive suspension system on an uneven road surface.* MECHANIKA.

11) *MRF-132DG Magneto-Rheological Fluid.* (2018, December 12). Retrieved from Mid- Atlantic Rubber- Magneto Rheological (MR Store):

http://www.lordmrstore.com/_literature_231215/Data_Sheet_-_MRF-132DG_Magneto-Rheological_Fluid

12) Premalata, S. E., Chokkalingam, R., & Mahendran, M. (2012). Magneto Mechanical Properties of Iron Based MR Fluids. *American Journal of Polymer Science*, 50-55.

13) Pritchard, P. J. (2011). *Fox and McDonald's Intoduction to Fluid Mechanics.* John Wiley & Sons, Inc.

14) Raghu, K. K., & Ramji, D. R. (2018). Study for Design of Magneto Rheological Damper. *Internation Journal on Recent and Innovation Trends in Computing and Communication*, 226-233.

15) Rao, S. (2011). *Mechanical Vibrations.* New Jersey: Prentice Hall.

16) Rill, G. (2012). *Road Vehicle Dynamics: Fundamentals and Modeling.* Boca Raton: CRC Press.

17) Roszkowski, A., Bogdan, M., Skoczynski, W., & Marek, B. (2008). Testing Viscosity of MR Fluid in Magnetic Field. *MEASUREMENT SCIENCE REVIEW*, 58-60.

18) Shames, I. H., & Cozzarelli, F. A. (2014). Elastic and Inelastic Stress Analysis. Boca Raton: Taylor & Francis Group.

19) Siramdasu, Y., & Taheri, S. (2017). *A New Semi-active Suspension System for Vehicle Applications.* Virginia: ASME.

20) Spencer Jr., B. F., Dyke, S. J., Sain, M. K., & Carlson, J. D. (1997). Phenomenological Model for Magnetorheological Dampers. *Journal of Engineering Mechanics*, 230-238.

21) Talbott, M. S., & Starkey, J. (2002). An Experimentally Validated Physical Model of a High- Performance Mono-Tube Damper. *SAE Motorsports Engineering Conference and Exhibition* (pp. P-382). Indiana: SAE.

22) Tyagi, S. (2016). *Development of a Semi-active Suspension System for Lighweight Automobiles.* VA.

23) Yao, G. Z., Yap, F. F., Chen, G., Li, W. H., & Yeo, S. H. (2002). MR damper and its application for semi-active control of vehicle suspension system. *Mechatronics*, 963-973.

PUBLICATIONS

Shrestha, K., Jha, A. K., & Luitel, M. C. (2019). Theoretical Study of Twin-tube Damper. *IOE Graduate Conference*.